Citation information: DOI: 10.1109/TNNLS.2024.3448376, IEEE Transactions on Neural Networks and Learning Systems

Nonfragile Impulsive State Estimation for Complex Networks With Markovian Switching Topologies Subject to Limited Bit Rate Constraints

Yuru Guo, Zidong Wang, *Fellow, IEEE*, Jun-Yi Li and Yong Xu, *Member, IEEE*

***Abstract*—In this paper, we consider the impulsive estimation problem for a specific category of discrete-time complex networks characterized by Markovian switching topologies. The measurement outputs of the underlying complex networks, transmitted to the observer over wireless networks, are subject to bit rate constraints. To effectively reduce the estimation error and enhance estimation performance, a mode-dependent impulsive observer is proposed that employs the impulse mechanism. The application of stochastic analysis techniques leads to the derivation of a sufficient condition for ensuring the mean-square boundedness of the estimation error dynamics. The upper bound of the error is then analyzed by iteratively exploring the Lyapunov relation at both impulsive and non-impulsive instants. Moreover, an optimization algorithm is presented for handling the bit rate allocation, which is coupled with the design of desired observer gains using the linear matrix inequality approach. Within this theoretical framework, the relationship between the mean-square estimation performance and the bit rate allocation protocol is further elucidated. Finally, a simulation example is provided to demonstrate the validity and effectiveness of the proposed impulsive estimation approach.**

***Index Terms*—Complex networks, state estimation, impulsive observer, bit rate constraint, Markovian switching topology.**

I. INTRODUCTION

Complex networks (CNs) are sophisticated systems consisting of numerous interconnected nodes linked by edges that represent relationships, interactions, or connections between nodes. These networks are prevalent in various natural, technological, and social systems including biological networks, transport networks, and social networks [1], [30], [34]. The widespread occurrence of CNs has spurred significant research into their estimation and control problems [9], [10], [15], [19], [36], [46]. Moreover, as CNs find increasingly diverse applications, additional characteristics such as jumping, uncertainties, and others are being recognized as crucial aspects to consider in CN studies.

The interactions among nodes in CNs can change over time due to various perturbations such as environmental influences, system failures, and reconfigurations, leading to switching topologies [13], [28]. Unlike static networks with fixed connections, dynamic networks with switching topologies have broader practical applications particularly in communication systems and power grids. Extensive research has been conducted in this area, focusing on control and state estimation problems [4], [37], [42]. For example, the nonfragile filtering problem for CNs has been addressed in [38], which employs Bernoulli distributed random variables to describe the switching topologies. In [24], the distributed filtering problem has been considered over sensor networks under Markovian switching topologies. The concept of semi-Markovian switching topologies has been expanded in [48] for the distributed estimation of sensor networks, with dwell time following an arbitrary probability distribution. Despite these advances, the exploration of Markovian switching topologies in CNs continues to be a dynamic and ongoing area of research.

In recent years, the field of impulsive control strategy has witnessed a significant surge in research, which shows its importance in the management of nonlinear dynamic systems [21], [26], [27], [33]. This strategy stands apart from traditional continuous-time control methods by introducing control inputs, termed impulse triggering instants, at specific discrete moments. Most current research in impulsive control concentrates on analyzing the dynamics of impulsive systems and developing impulsive controllers, where the core objective of incorporating the impulse mechanism in controller design is to optimize the use of network resources and reduce control costs [14], [35]. Nevertheless, the area of impulsive estimation has not been as extensively explored. As the dual problem to impulsive control, impulsive estimation offers a rich avenue for investigation, which promises to contribute significantly to the understanding of dynamic systems.

The concept of an impulsive observer is characterized by the use of an impulsive update strategy and can be divided into two main categories. The first category includes observers that update their estimates only when measurements are received at discrete time-instants over a network [6], [16], [31]. This approach contrasts with continuously updated observers and is notable for its significant conservation of network resources.

This work was supported in part by the Natural Science Foundation of Guangdong Province of China under Grants 2021B0101410005, 2021A1515011634 and 2021B1515420008, the National Natural Science Foundation of China under Grants U22A2044 and 62206063, the Key Area Research and Development Program of Guangdong Province of China under Grant 2021B0101410005, the Local Innovative and Research Teams Project of Guangdong Special Support Program of China under Grant 2019BT02X353, and the China Scholarship Council under Grant 202208440312. *(Corresponding author: Jun-Yi Li)*

Yuru Guo, Jun-Yi Li and Yong Xu are with the Guangdong-Hong Kong Joint Laboratory for Intelligent Decision and Cooperative Control, Guangdong Provincial Key Laboratory of Intelligent Decision and Cooperative Control, School of Automation, Guangdong University of Technology, Guangzhou 510006, China. Jun-Yi Li is also with the Pazhou Lab, Guangzhou 510330, China. (E-mails: guo_yuru0626@163.com; jun-yi-li@foxmail.com; yxu@gdut.edu.cn)

Zidong Wang is with the Department of Computer Science, Brunel University London, Uxbridge UB8 3PH, United Kingdom. (E-mail: Zidong.Wang@brunel.ac.uk)

This article has been accepted for publication in a future issue of this journal, but has not been fully edited. Content may change prior to final publication.
Citation information: DOI: 10.1109/TNNLS.2024.3448376, IEEE Transactions on Neural Networks and Learning Systems

The second category encompasses impulsive re-update observers [29], [45], which enhance the convergence rate of the observer by incorporating an impulsive strategy into the traditional observer framework. A key point to note is that all the mentioned works have been formulated within the continuous-time framework [22]. In discrete-time systems, the absence of left-limits and right-limits introduces unique challenges for impulsive analysis. Up to now, discrete-time impulsive control methods have been addressed in some prior works [7], [12], which lay a foundation for further research. Despite these developments, the integration of impulse mechanisms into observer development within a discrete-time framework remains an underexplored area.

The focus of state estimation approaches has historically been on continuous-time CNs within analog communication frameworks. However, the rapid progression in digital network technology has catalyzed a shift in communication mechanisms for control systems [3]. Traditional analog communication methods, once prevalent, are increasingly seen as insufficient for the evolving demands of modern control systems. In place of analog methods, digital communication strategies have risen to prominence. These digital approaches offer significant benefits over analog methods, including enhanced robustness, increased reliability, and improved energy efficiency [23]. Yet, the realm of research that specifically addresses the challenges of control and estimation in CNs utilizing digital communication networks is still somewhat limited.

Bit rate, which is a key factor in wireless digital networks, defines the amount of data that can be transmitted through these networks within a specific time frame [2], [8], [25]. A higher bit rate typically allows for more data to be sent over digital networks per second, thereby enhancing communication efficiency and response times. Unfortunately, in practical scenarios, bit rate often faces limitations due to conditions like wireless channel constraints and limited bandwidth availability. These restrictions present significant challenges in ensuring fast and reliable data transmission in wireless digital networks [44]. Given these challenges, strategic allocation of bit rates becomes essential to optimize resource utilization among multiple nodes in a network [5]. Exploring the intricacies of bit rate constraints and allocation protocols is vital for understanding system dynamics within the context of wireless digital networks.

The coding-decoding procedure in wireless digital networks plays a crucial role in facilitating data exchange among devices [43], [47]. This process involves a series of operations, namely, sampling, quantization, and coding, that convert the analog signal into a digital format. Initially, in the sampling and quantization phases, the analog signal is transformed into a discrete representation, and this is followed by a coding process, which maps the discrete representation into specific code words represented by binary values 0 and 1. This crucial mapping transforms the original data into a bit sequence for digital transmission, thereby enabling efficient data transmission over digital networks [40]. During the decoding phase, the received digital data is converted back into analog signals. However, due to the limited bit rates in the network, the accuracy of this decoding is often compromised, leading to errors in the coding process. These errors can significantly affect the overall system performance. Given these challenges, the need for in-depth research into estimation for CNs under bit rate constraints becomes evident.

Motivated by the above discussions, the focus of our study is on addressing the state estimation problem for CNs with Markovian switching topologies by using an impulsive method under constrained bit rate conditions. This problem presents three main challenges: i) *the development of a nonfragile impulsive observer*, which involves creating an impulsive observer that effectively integrates Markovian switching modes with impulse triggering instants within a discrete-time framework, ensuring it remains robust against system variations; ii) *the assurance of stability under bit-rate constraints*, where the challenge is to maintain the stability of the impulsive error dynamics despite bit-rate limitations, and also to establish a link between bit-rate allocation and estimation performance; and iii) *the design of impulsive observer gain*, where the goal is to achieve bounded state estimation under the bit-rate constraints, which demands innovative approaches to balance gain effectiveness and communication limitations.

In response to the identified challenges, the key contributions of our study are summarized as follows.

1) The state estimation issue is addressed, for the first time, for discrete-time CNs featuring Markovian switching topologies within digital communication networks, where the bit rate constraints are considered as a reflection of inherent bandwidth limitations in such networks.
2) A mode-dependent impulsive observer is devised for the state estimation of CNs, and a sufficient condition is established to ensure the mean-square boundedness of the impulsive error dynamics. Furthermore, the upper bound on the estimation error is meticulously analyzed by incorporating energy functions between impulsive and non-impulsive instants.
3) The relationship between estimation performance and bit rate allocation is established, in the context of the impulsive mechanism, by introducing a collaborative optimization algorithm designed to efficiently allocate bit rates while simultaneously fine-tuning the impulsive observer gains for optimal performance.

The structure of this work is organized as follows. Section II provides a comprehensive description of the models used in the study, which includes details on discrete-time CNs with Markovian switching topologies, the specifics of network transmission under bit rate constraints, the structure of the adopted impulsive observer, and an overview of the impulsive error dynamics. Section III is focused on the analytical aspects of the study, which covers the analysis of the boundedness of estimation error, the methodology for designing observer gains, and a collaborative approach for the co-design of bit rate allocation and the observer gains. In Section IV, a numerical example is provided to demonstrate the practical application and validate the correctness of the theoretical results derived in the study. This section also includes explanatory notes to aid in understanding the example. Section V serves as the

Citation information: DOI: 10.1109/TNNLS.2024.3448376, IEEE Transactions on Neural Networks and Learning Systems

conclusion to this paper.

Notations: Through this article, we define the representation of some symbols. Symbols $\mathbb{R}^m$, $\mathbb{R}^{m\times n}$, $\mathbb{N}$, and $\mathbb{N}^+$ represent the m-dimensional Euclidean space, the $m \times n$ real matrices, the non-negative integers, and the positive integers, respectively. The symbol $\|\cdot\|$ refers to the Euclidean norm, and $|\cdot|$ stands for the absolute value. The expectation of a stochastic variable is depicted by $\mathbb{E}\cdot$. For a matrix X, its transpose is denoted by X^T, and $\underline{\lambda}(X)$ signifies its minimum eigenvalue. A column vector is expressed by $\mathrm{col}\cdot$. The diagonal matrix is articulated as $\mathrm{diag}\cdots$. The Kronecker product is represented by the symbol $\otimes$, and I denotes the identity matrix with proper dimensions.

II. Problem Formulation and Preliminaries

A. Complex Networks With Markovian Switching Topologies

Consider a class of CNs with Markovian switching topologies represented by

$$\begin{cases} x_\jmath(k) = A_\jmath x_\jmath(k-1) + B_\jmath f(x_\jmath(k-1)) \\ \qquad + \sum_{\ell=1}^{N} \omega_{\jmath\ell}^{\sigma(k-1)} \Gamma x_\ell(k-1) + S_\jmath \upsilon(k-1) \\ y_\jmath(k) = C_\jmath x_\jmath(k) + M_\jmath \upsilon(k) \end{cases} \tag{1}$$

where $x_\jmath(k) \in \mathbb{R}^{n_x}$ and $y_\jmath(k) \in \mathbb{R}^{n_y}$ $\big(\jmath \in \mathcal{J} \triangleq \{1, 2, \ldots, N\}\big)$ denote the state and the measurement output of node $\jmath$, respectively; $A_\jmath$, $B_\jmath$, $S_\jmath$, $C_\jmath$, and $M_\jmath$ are known matrices with appropriate dimensions; $f(x_\jmath(k)) \in \mathbb{R}^{n_x}$ is a nonlinear function that will be introduced later; the vector $\upsilon(k) \in \mathbb{R}^{n_\upsilon}$ is the external noise meeting $\|\upsilon(k)\| \le \bar{\upsilon}$; the inner coupling matrix $\Gamma \triangleq \mathrm{diag}\{r_1, r_2, \ldots, r_{n_x}\}$ represents the relationship between each element of state vector and different nodes, and $r_\varsigma \ne 0$ means that the ς-th element of the state of node ℓ has an effect on node $\jmath$; the matrix $W^{\sigma(k)} \triangleq \Big(\omega_{\jmath\ell}^{\sigma(k)}\Big) \in \mathbb{R}^{N\times N}$ indicates the outer coupling configuration with the mode switching, which satisfies the following condition:

$$\omega_{\jmath\jmath}^{\sigma(k)} = -\sum_{\ell=1,\ell\ne\jmath}^{N} \omega_{\jmath\ell}^{\sigma(k)}, \ \forall \jmath, \ell \in \mathcal{J}.$$

Here, $\omega_{\jmath\ell}^{\sigma(k)} > 0$ means that the node ℓ can receive signals from the node $\jmath$, otherwise, $\omega_{\jmath\ell}^{\sigma(k)} = 0$, and $\sigma(k)$ is a discrete-time homogeneous Markov chain taking values in a finite set $\Pi \triangleq \{1, 2, \ldots, \tau\}$. The transition probability matrix $\Theta \triangleq (\theta_{ij}) \in \mathbb{R}^{\tau\times\tau}$ is given by

$$\mathbb{P}\{\sigma(k) = j | \sigma(k-1) = i\} = \theta_{ij}, \ \forall i, j \in \Pi \tag{2}$$

where $\theta_{ij} \ge 0$ and $\sum_{j=1}^{\tau} \theta_{ij} = 1$.

The nonlinear function $f(x_\jmath(k))$ satisfies the following assumption.

Assumption 1: The nonlinear function $f(\cdot) \in \mathbb{R}^{n_x}$ meets the following condition:

$$\big(f(a) - f(b) - \psi_1(a-b)\big)^T \\ \times \big(f(a) - f(b) - \psi_2(a-b)\big) \le 0$$

where $a, b \in \mathbb{R}^{n_x}$ are some vectors, and $\psi_1 \in \mathbb{R}^{n_x\times n_x}$ and $\psi_2 \in \mathbb{R}^{n_x\times n_x}$ are known matrices.

B. Transmission Over Bit Rate Constrained Network

The analog signals obtained from the sensors must undergo conversion into digital signals within the coder, to facilitate the transmission over digital network. In practice, the bandwidth of wireless communication network is often limited, which means that the number of bits allowed to be transmitted at each time instant is restricted. Allocating the appropriate bit rate for each node can effectively avoid data collisions during transmission in the wireless network. We assume that the total available bit rates of entire network are U ($U \in \mathbb{N}$). Measurement $y_\jmath(k)$ of each node in the CNs is transmitted over the bit-rate constrained wireless network, and the bit rate allocated to each sensor adheres to the following condition [18]

$$U \ge \sum_{\jmath=1}^{N} U_\jmath, \ U_\jmath \in \mathbb{N} \tag{3}$$

where $U_\jmath$ ($\jmath \in \mathcal{J}$) denotes the bit rate allocated to the node $\jmath$, that is, each coder has limited bit rates to encode the data packet. As a result, the data compression is required, which can be realized by a uniform quantizer. To be specific, this quantizer segments the quantization region into a set number of uniformly spaced intervals. The quantization process involves mapping each input data to its corresponding interval. The quantization level $q_\jmath$ (denoting the number of intervals) of the node $\jmath$ is limited by the allocated bits, which satisfies

$$q_\jmath \le \hat{q}_\jmath = \left\lfloor \sqrt[n_y]{2^{U_\jmath}} \right\rfloor \tag{4}$$

where the symbol $\lfloor\cdot\rfloor$ stands for rounding down function.

Given a scalar $\delta_\jmath > 0$ depicting the upper bound of the quantization region, one has

$$|y_{\jmath,\kappa}(k)| \le \delta_\jmath, \ \forall \kappa \in \{1, 2, \ldots, n_y\} \tag{5}$$

where $y_{\jmath,\kappa}(k)$ represents the κ-th element of the measurement $y_\jmath(k)$.

Choosing a quantization level $q_\jmath$ for the node $\jmath$, the quantization region is uniformly segmented into some sub-hyperrectangles as follows:

$$\mathcal{Q}_{\jmath,\kappa}^{(1)}(\delta_\jmath) \triangleq \left\{ y_{\jmath,\kappa}(k) \middle| -\delta_\jmath \le y_{\jmath,\kappa}(k) < -\delta_\jmath + \frac{2\delta_\jmath}{q_\jmath} \right\}$$
$$\mathcal{Q}_{\jmath,\kappa}^{(2)}(\delta_\jmath) \triangleq \left\{ y_{\jmath,\kappa}(k) \middle| -\delta_\jmath + \frac{2\delta_\jmath}{q_\jmath} \le y_{\jmath,\kappa}(k) < -\delta_\jmath + \frac{4\delta_\jmath}{q_\jmath} \right\}$$
$$\vdots$$
$$\mathcal{Q}_{\jmath,\kappa}^{(q_\jmath)}(\delta_\jmath) \triangleq \left\{ y_{\jmath,\kappa}(k) \middle| \delta_\jmath - \frac{2\delta_\jmath}{q_\jmath} \le y_{\jmath,\kappa}(k) \le \delta_\jmath \right\}.$$

A string of integers $\{d_{\jmath,1}, d_{\jmath,2}, \ldots, d_{\jmath,n_y}\} \in \{1, 2, \ldots, q_\jmath\}$ represents the quantization region corresponding to each element of the node $\jmath$. Then, the coder $\jmath$ encodes this string of integers using binary representation, namely 0 and 1, and outputs the binary codeword $\tilde{Y}_\jmath(k) \triangleq \aleph\big(\{d_{\jmath,1}, d_{\jmath,2}, \ldots, d_{\jmath,n_y}\}\big)$, where $\aleph(\cdot)$ denotes the coding function.

The binary codeword $\tilde{Y}_\jmath(k)$ is transmitted over the wireless communication network to the decoder $\jmath$ by utilizing the same network transmission protocol according to the coder $\jmath$. After

This article has been accepted for publication in a future issue of this journal, but has not been fully edited. Content may change prior to final publication.
Citation information: DOI: 10.1109/TNNLS.2024.3448376, IEEE Transactions on Neural Networks and Learning Systems

decoding, the central values $\{s_{\jmath,1}, s_{\jmath,2}, \ldots, s_{\jmath,n_y}\}$ of the sub-hyperrectangles are used to approximate the original data, which is computed by

$$s_{\jmath,\kappa} = -\delta_\jmath + \frac{(2d_{\jmath,\kappa}-1)\delta_\jmath}{\hat{q}_\jmath},\ \kappa \in \{1,2,\ldots,n_y\}. \tag{6}$$

Based on the above analysis, the quantization error of the measurement $y_\jmath(k)$ satisfies

$$\left\| y_\jmath(k) - \begin{bmatrix} s_{\jmath,1} & s_{\jmath,2} & \ldots & s_{\jmath,n_y} \end{bmatrix}^T \right\|_2 \leq \frac{\sqrt{n_y}\delta_\jmath}{\hat{q}_\jmath}. \tag{7}$$

Denoting the decoding output as

$$\vec{y}_\jmath(k) \triangleq \begin{bmatrix} s_{\jmath,1} & s_{\jmath,2} & \ldots & s_{\jmath,n_y} \end{bmatrix}^T,$$

the decoding error is obtained as

$$\phi_\jmath(k) \triangleq y_\jmath(k) - \vec{y}_\jmath(k). \tag{8}$$

Remark 1: In wireless communication networks, bit rate allocation follows either dynamic or static protocols. Dynamic protocols adapt bit rates to the fluctuating needs of user devices, enhancing individual data transmission efficiency. Static protocols, in contrast, allocate bit rates based on pre-set criteria, ideal for scenarios with multiple users sharing limited bandwidth, aiming for equitable data transmission. This study employs a static bit rate allocation protocol within CNs to ensure consistent and fair distribution of bandwidth among all network nodes.

C. Observer With Impulsive Dynamical Behavior

To estimate the internal state of system efficiently utilizing the decoded measurement output, we introduce an impulsive observer as follows:

$$\begin{cases} \hat{x}_\jmath(k) = A_\jmath \hat{x}_\jmath(k-1) + \sum_{\jmath=1}^{N} \omega_{\jmath\ell}^{\sigma(k-1)} \Gamma \hat{x}_\ell(k-1) \\ \qquad + B_\jmath f(\hat{x}_\jmath(k-1)) + \left(L_\jmath^{\sigma(k-1)} + \Delta L_\jmath(k-1)\right) \\ \qquad \times \left(\vec{y}_\jmath(k-1) - C_\jmath \hat{x}_\jmath(k-1)\right), k \in (k_{\epsilon-1}, k_\epsilon] \\ \hat{x}_\jmath^+(k_\epsilon) = \hat{x}_\jmath(k) + K_\jmath^{\sigma(k-1)}\left(\vec{y}_\jmath(k) - C_\jmath \hat{x}_\jmath(k)\right), k = k_\epsilon \\ \hat{x}_\jmath^+(k_0) = \hat{x}_\jmath(0) \end{cases} \tag{9}$$

where $\hat{x}_\jmath(k)$ denotes the state estimate for node $\jmath$; $L_\jmath^{\sigma(k)}$ and $K_\jmath^{\sigma(k)}$ represent the mode-dependent gain matrices to be designed; and the real matrix $\Delta L_\jmath(k)$ denotes the observer gain variation given as follows:

$$\Delta L_\jmath(k) = D_\jmath Q_\jmath(k) H_\jmath \tag{10}$$

where $D_\jmath$ and $H_\jmath$ are constant matrices, and $Q_\jmath(k)$ is the time-varying uncertain matrix satisfying $Q_\jmath^T(k) Q_\jmath(k) \leq I$.

The integer sequence $\{k_\epsilon\}$ represents the impulse triggering instants with $\epsilon \in \mathbb{N}^+$, which is monotonically increasing, i.e., $k_0 = 0 < k_1 < \ldots < k_\epsilon < \ldots$ with $\lim_{\epsilon\to\infty} k_\epsilon = \infty$. The observer proposed in (9) distinguishes itself from a classical observer through the inclusion of an additional update, denoted as $\hat{x}_\jmath^+(k_\epsilon)$. This update occurs at specific impulse triggering instants, labeled as k_ϵ, at which the observer's dynamics experience an abrupt change, and such a change is characteristic of impulsive dynamical behavior. The term $\hat{x}_\jmath^+(k_\epsilon)$ is used to represent the state of the observer immediately after it has been influenced by an impulse signal, reflecting the immediate effect of the impulsive update on the observer's state.

The interval of the impulse sequence determines the frequency of the observer's impulsive update. Define the interval between adjacent impulse instants as $\hbar_\epsilon \triangleq k_\epsilon - k_{\epsilon-1}$, which satisfies the following assumption.

Assumption 2: [7] The interval $\hbar_\epsilon \in \mathbb{N}^+$ between adjacent impulse triggering instants satisfies

$$0 < \hbar_\epsilon \leq \tilde{\hbar},\ \epsilon \in \mathbb{N}^+ \tag{11}$$

where the integer $\tilde{\hbar} \geq 1$ is a given upper bound.

Remark 2: Reviewing the impulsive observer (9), the correction terms are

$$\left(L_\jmath^{\sigma(k-1)} + \Delta L_\jmath(k-1)\right)\left(\vec{y}_\jmath(k-1) - C_\jmath \hat{x}_\jmath(k-1)\right),$$

and

$$K_\jmath^{\sigma(k-1)}\left(\vec{y}_\jmath(k) - C_\jmath \hat{x}_\jmath(k)\right)\nabla(k-k_\epsilon)$$

where $\nabla(k-k_\epsilon)$ is the Dirac impulse function meeting $\nabla(k-k_\epsilon) = 1$ when $k = k_\epsilon$, otherwise, $\nabla(k-k_\epsilon) = 0$. For $K_\jmath^{\sigma(k-1)} = 0$, the observer (9) becomes a classical nonfragile observer.

Remark 3: Existing research on impulsive observers predominantly centers around continuous-time systems, with relatively scant attention given to their discrete-time counterparts. Furthermore, there is a noticeable gap in studies focusing on impulsive observers with Markovian mode-dependent characteristics. To summarize, the bulk of current research in the impulsive estimation domain typically revolves around state estimation in impulsive systems [20] or impulsive estimation due to discrete measurement outputs in continuous-time systems [31]. In this work, we take a pioneering step by introducing a discrete-time impulsive observer that adeptly manages the interplay between Markovian switching topologies and impulsive triggering instants. This innovative approach utilizes the impulse mechanism to actively reduce estimation errors and enhance overall estimation performance.

D. Impulsive Error Dynamics

Define $e_\jmath(k) \triangleq x_\jmath(k) - \hat{x}_\jmath(k)$ as the estimation error. At the non-impulsive triggering interval $k \in (k_{\epsilon-1}, k_\epsilon]$, we have the following error dynamics:

$$\begin{aligned} e_\jmath(k) = {} & A_\jmath e_\jmath(k-1) + \sum_{\jmath=1}^{N} \omega_{\jmath\ell}^{\sigma(k-1)} \Gamma e_\ell(k-1) \\ & + B_\jmath \tilde{f}(e_\jmath(k-1)) - \left(L_\jmath^{\sigma(k-1)} + \Delta L_\jmath(k-1)\right) \\ & \times \left(\vec{y}_\jmath(k-1) - C_\jmath \hat{x}_\jmath(k-1)\right) + S_\jmath \upsilon(k-1) \end{aligned} \tag{12}$$

where $\tilde{f}(e_\jmath(k)) \triangleq f(x_\jmath(k)) - f(\hat{x}_\jmath(k))$. At the impulsive time instants, the error dynamics evolves as

$$\begin{aligned} e_\jmath^+(k_\epsilon) = {} & x_\jmath(k_\epsilon) - \hat{x}_\jmath^+(k_\epsilon) \\ = {} & e_\jmath(k_\epsilon) - K_\jmath^{\sigma(k-1)}\left(\vec{y}_\jmath(k_\epsilon) - C_\jmath \hat{x}_\jmath(k_\epsilon)\right). \end{aligned} \tag{13}$$

This article has been accepted for publication in a future issue of this journal, but has not been fully edited. Content may change prior to final publication.
Citation information: DOI: 10.1109/TNNLS.2024.3448376, IEEE Transactions on Neural Networks and Learning Systems

Define the augmented error vector as

$$e(k) \triangleq \begin{bmatrix} e_1^T(k) & e_2^T(k) & \dots & e_N^T(k) \end{bmatrix}^T.$$

Combining the decoding error (8) with the estimation error, the augmented error dynamics is presented by

$$\begin{aligned} e(k) =& Ae(k-1) + B\mathcal{F}(e(k-1)) + Sv(k-1) \\ &+ \left(W^{\sigma(k-1)} \otimes \Gamma\right) e(k-1) - \big(L^{\sigma(k-1)} \\ &+ \Delta L(k-1)\big)\big(Ce(k-1) + Mv(k-1) \\ &- \Phi(k-1)\big) \\ =& \Omega_1^{\sigma(k-1)} e(k-1) + B\mathcal{F}(e(k-1)) + \Omega_2^{\sigma(k-1)} \\ &\times v(k-1) + \Omega_3^{\sigma(k-1)} \Phi(k-1), k \in (k_{\epsilon-1}, k_\epsilon], \end{aligned} \tag{14}$$

and

$$\begin{aligned} e^+(k_\epsilon) =& \Omega_4^{\sigma(k-1)} e(k_\epsilon) - K^{\sigma(k-1)} Mv(k_\epsilon) \\ &+ K^{\sigma(k-1)} \Phi(k_\epsilon) \end{aligned} \tag{15}$$

where

$$\begin{aligned} A &\triangleq \operatorname{diag}\{A_1, A_2, \dots, A_N\}, \\ B &\triangleq \operatorname{diag}\{B_1, B_2, \dots, B_N\}, \\ C &\triangleq \operatorname{diag}\{C_1, C_2, \dots, C_N\}, \\ M &\triangleq \operatorname{col}\{M_1, M_2, \dots, M_N\}, \\ S &\triangleq \operatorname{col}\{S_1, S_2, \dots, S_N\}, \\ D &\triangleq \operatorname{diag}\{D_1, D_2, \dots, D_N\}, \\ H &\triangleq \operatorname{diag}\{H_1, H_2, \dots, H_N\}, \\ K^{\sigma(k)} &\triangleq \operatorname{diag}\{K_1^{\sigma(k)}, K_2^{\sigma(k)}, \dots, K_N^{\sigma(k)}\}, \\ L^{\sigma(k)} &\triangleq \operatorname{diag}\{L_1^{\sigma(k)}, L_2^{\sigma(k)}, \dots, L_N^{\sigma(k)}\}, \\ \Omega_1^{\sigma(k)} &\triangleq A + W^{\sigma(k)} \otimes \Gamma - \big(L^{\sigma(k)} + \Delta L(k)\big)C, \\ \Omega_2^{\sigma(k)} &\triangleq S - \big(L^{\sigma(k)} + \Delta L(k)\big)M, \\ \Omega_4^{\sigma(k)} &\triangleq I - K^{\sigma(k)} C, \ \Delta L(k) \triangleq DQ(k)H, \\ \Omega_3^{\sigma(k)} &\triangleq L^{\sigma(k)} + \Delta L(k), \\ Q(k) &\triangleq \operatorname{diag}\{Q_1(k), Q_2(k), \dots, Q_N(k)\}, \\ \Phi(k) &\triangleq \operatorname{col}\{\phi_1(k), \phi_2(k), \dots, \phi_N(k)\}, \\ \mathcal{F}(e(k)) &\triangleq \begin{bmatrix} \tilde{f}^T(e_1(k)) & \tilde{f}^T(e_2(k)) & \dots & \tilde{f}^T(e_N(k)) \end{bmatrix}^T. \end{aligned}$$

The following lemma and definition are introduced to facilitate the subsequent analysis.

Lemma 1: [39] For given real matrices $R_1 = R_1^T$, R_2 and R_3, and $Q(k)$ with $Q^T(k)Q(k) \le I$. The following relationship

$$R_1 + R_3 Q(k) R_2 + R_2^T Q^T(k) R_3^T < 0$$

holds if and only if there exists a scalar $\gamma > 0$ such that

$$R_1 + \gamma R_2^T R_2 + \frac{1}{\gamma} R_3 R_3^T < 0.$$

Definition 1: [41] The augmented error dynamics is said to be exponentially mean-square bounded if there exist constants $|a| < 1$, $b > 0$ and $c > 0$ such that the following inequality holds:

$$\mathbb{E}\{\|e(k)\|^2\} \le a^k b + c \tag{16}$$

where c is an asymptotic upper bound of the error $\mathbb{E}\{\|e(k)\|^2\}$.

The main objective of this work is to develop an impulsive observer for the complex networks in the context of digital communication networks such that the impulsive error dynamics is ultimately bounded subject to the exponential stability analysis methods.

III. Main Result

A. Boundedness Analysis

In the following theorem, a sufficient condition is given to analyze the exponential boundedness in the mean-square sense of the augmented error dynamics.

For facilitating the analysis, we denote

$$\begin{aligned} &\tilde{\mathcal{P}}_{(i)} \triangleq \sum_{j=1}^{\tau} \theta_{ij} \mathcal{P}^{(j)}, \ \mathcal{P}^{(i)} \triangleq \operatorname{diag}\left\{P_1^{(i)}, P_2^{(i)}, \dots, P_N^{(i)}\right\}, \\ &\Lambda_1 \triangleq \gamma_1 \Psi_1^T \Psi_2, \ \Lambda_2 \triangleq -\gamma_1 \frac{\Psi_1^T + \Psi_2^T}{2}, \\ &\Psi_1 \triangleq I \otimes \psi_1, \ \Psi_2 \triangleq I \otimes \psi_2. \end{aligned}$$

Theorem 1: Consider the CN (1) and the impulsive observer (9) with the known positive integers $U_\jmath$, the given scalars $\rho_1 > 0$, $0 < \rho_2 < 1$, $\tilde{\hbar} \ge 1$, and the observer gain matrices $L_\jmath^{(i)}$ and $K_\jmath^{(i)}$ ($\jmath \in \mathcal{J}$). Then, the estimation error dynamics is exponentially mean-square bounded if there exist positive scalars $\gamma_\iota > 0$ ($\iota \in \{1, 2, \dots, 5\}$), and positive definite matrices $P_\jmath^{(i)}$ ($\jmath \in \mathcal{J}$) such that the following inequalities hold for all $i \in \Pi$:

$$\begin{bmatrix} -\rho_1 \mathcal{P}^{(i)} - \Lambda_1 & -\Lambda_2 & 0 & 0 & \left(\Omega_1^{(i)}\right)^T \\ * & -\gamma_1 I & 0 & 0 & B^T \\ * & * & -\gamma_2 I & 0 & \left(\Omega_2^{(i)}\right)^T \\ * & * & * & -\gamma_3 I & \left(\Omega_3^{(i)}\right)^T \\ * & * & * & * & -\tilde{\mathcal{P}}_{(i)}^{-1} \end{bmatrix} < 0 \tag{17}$$

$$\begin{bmatrix} -\rho_2 \tilde{\mathcal{P}}_{(i)} & 0 & 0 & \left(\Omega_4^{(i)}\right)^T \\ * & -\gamma_4 I & 0 & -M^T \left(K^{(i)}\right)^T \\ * & * & -\gamma_5 I & \left(K^{(i)}\right)^T \\ * & * & * & -\tilde{\mathcal{P}}_{(i)}^{-1} \end{bmatrix} < 0 \tag{18}$$

$$0 < \rho_1^{\tilde{\hbar}} \rho_2 < 1. \tag{19}$$

Proof: Choose the following Lyapunov-like function for the stability analysis:

$$\mathcal{V}(k) = e^T(k) \mathcal{P}^{\sigma(k)} e(k). \tag{20}$$

Denote $\sigma(k) \triangleq \jmath$, $\sigma(k-1) \triangleq i$, and define an augmented vector as

$$\zeta(k) \triangleq \begin{bmatrix} e^T(k) & \mathcal{F}^T(e(k)) & v^T(k) & \Phi^T(k) \end{bmatrix}^T.$$

Then, the error dynamics is analyzed in the following two steps.

Step 1: For the intervals $(k_{\epsilon-1}, k_\epsilon]$ ($\epsilon \in \mathbb{N}^+$) without impulse effect, the mathematical expectation of the difference equation is given as

$$\begin{aligned}\Delta\mathcal{V}(k) \triangleq& \mathbb{E}\{\mathcal{V}(k)|\mathcal{V}(k-1)\} - \rho_1\mathcal{V}(k-1)\\ =&\zeta^T(k-1)\Xi\zeta(k-1) + \gamma_2\upsilon^T(k-1)\\ &\times \upsilon^T(k-1) + \gamma_3\Phi^T(k-1)\Phi^T(k-1) \end{aligned}\tag{21}$$

where

$$\Xi \triangleq \begin{bmatrix}\Xi_{11} & \Xi_{12} & \Xi_{13} & \Xi_{14}\\ * & \Xi_{22} & \Xi_{23} & \Xi_{24}\\ * & * & \Xi_{33} & \Xi_{34}\\ * & * & * & \Xi_{44}\end{bmatrix},$$

$$\begin{aligned}\Xi_{11} \triangleq& \big(\Omega_1^{(i)}\big)^T\tilde{\mathcal{P}}_{(i)}\Omega_1^{(i)} - \rho_1\mathcal{P}^{(i)},\\ \Xi_{12} \triangleq& \big(\Omega_1^{(i)}\big)^T\tilde{\mathcal{P}}_{(i)}B,\ \Xi_{13} \triangleq \big(\Omega_1^{(i)}\big)^T\tilde{\mathcal{P}}_{(i)}\Omega_2^{(i)},\\ \Xi_{14} \triangleq& \big(\Omega_1^{(i)}\big)^T\tilde{\mathcal{P}}_{(i)}\big(L^{(i)} + \Delta L(k-1)\big),\\ \Xi_{22} \triangleq& B^T\tilde{\mathcal{P}}_{(i)}B,\ \Xi_{23} \triangleq B^T\tilde{\mathcal{P}}_{(i)}\Omega_2^{(i)},\\ \Xi_{24} \triangleq& B^T\tilde{\mathcal{P}}_{(i)}\big(L^{(i)} + \Delta L(k-1)\big),\\ \Xi_{33} \triangleq& \big(\Omega_2^{(i)}\big)^T\tilde{\mathcal{P}}_{(i)}\Omega_2^{(i)} - \gamma_2 I,\\ \Xi_{34} \triangleq& \big(\Omega_2^{(i)}\big)^T\tilde{\mathcal{P}}_{(i)}\big(L^{(i)} + \Delta L(k-1)\big),\\ \Xi_{44} \triangleq& \big(L^{(i)} + \Delta L(k-1)\big)^T\tilde{\mathcal{P}}_{(i)}\\ &\times \big(L^{(i)} + \Delta L(k-1)\big) - \gamma_3 I.\end{aligned}$$

From Assumption 1, we know that the nonlinearity $f(\cdot)$ fulfills

$$\big(\mathcal{F}(e(k)) - \Psi_1 e(k)\big)^T\big(\mathcal{F}(e(k)) - e(k)\Psi_2\big) \le 0, \tag{22}$$

which can be further expressed as

$$\begin{bmatrix} e(k)\\ \mathcal{F}(e(k))\end{bmatrix}^T \begin{bmatrix}\gamma_1\Psi_1^T\Psi_2 & -\gamma_1\frac{\Psi_1^T+\Psi_2^T}{2}\\ * & \gamma_1 I\end{bmatrix}\begin{bmatrix} e(k)\\ \mathcal{F}(e(k))\end{bmatrix} \le 0 \tag{23}$$

for any scalar $\gamma_1 > 0$.

Combining (21) with (23), one has

$$\begin{aligned}\Delta\mathcal{V}(k) =&\zeta^T(k-1)\tilde{\Xi}\zeta(k-1) + \gamma_2\upsilon^T(k-1)\\ &\times \upsilon^T(k-1) + \gamma_3\Phi^T(k-1)\Phi^T(k-1)\end{aligned}\tag{24}$$

where

$$\tilde{\Xi} \triangleq \begin{bmatrix}\Xi_{11}-\Lambda_1 & \Xi_{12}-\Lambda_2 & \Xi_{13} & \Xi_{14}\\ * & \Xi_{22}-\gamma_1 I & \Xi_{23} & \Xi_{24}\\ * & * & \Xi_{33} & \Xi_{34}\\ * & * & * & \Xi_{44}\end{bmatrix}.$$

Applying the Schur Complement Lemma [17] to the above formula, one has $\tilde{\Xi} < 0$ based on the condition (17) in Theorem 1. Then, we derive that

$$\Delta\mathcal{V}(k) <\gamma_2\upsilon^T(k-1)\upsilon^T(k-1) + \gamma_3\Phi^T(k-1)\Phi^T(k-1). \tag{25}$$

Taking the mathematical expectation of (25), and recalling the decoding error (8) and the definition of the external noise, the following relation is obtained:

$$\mathbb{E}\{\mathcal{V}(k)\} <\rho_1\mathbb{E}\{\mathcal{V}(k-1)\} + \mu_1 \tag{26}$$

where

$$\mu_1 \triangleq \gamma_2\bar{\upsilon}^2 + \gamma_3\sum_{\jmath=1}^{N}\frac{n_y\delta_\jmath^2}{\lfloor\sqrt[n_y]{2^{U_\jmath}}\rfloor^2}.$$

Step 2: At the impulse triggering instants $k = k_\epsilon$ ($\epsilon \in \mathbb{N}^+$), a prominent impulsive jump with the form (15) occurs in the error dynamics $e^+(k_\epsilon)$. Denoting

$$\begin{aligned}\Delta\mathcal{V}^+(k_\epsilon) &\triangleq \mathbb{E}\{\mathcal{V}^+(k_\epsilon)|\mathcal{V}(k_\epsilon)\} - \rho_2\mathcal{V}(k_\epsilon),\\ \hat{\zeta}(k) &\triangleq \begin{bmatrix}e^T(k) & \upsilon^T(k) & \Phi^T(k)\end{bmatrix}^T,\end{aligned}$$

one obtains

$$\begin{aligned}\Delta\mathcal{V}^+(k_\epsilon) =&\hat{\zeta}^T(k_\epsilon)\begin{bmatrix}\hat{\Xi}_{11} & \hat{\Xi}_{12} & \hat{\Xi}_{13}\\ * & \hat{\Xi}_{22} & \hat{\Xi}_{23}\\ * & * & \hat{\Xi}_{33}\end{bmatrix}\hat{\zeta}(k_\epsilon)\\ &+ \gamma_4\upsilon^T(k_\epsilon)\upsilon^T(k_\epsilon) + \gamma_5\Phi^T(k_\epsilon)\Phi^T(k_\epsilon)\end{aligned}\tag{27}$$

where

$$\begin{aligned}\hat{\Xi}_{11} \triangleq& \big(\Omega_4^{(i)}\big)^T\tilde{\mathcal{P}}_{(i)}\Omega_4^{(i)} - \rho_2\tilde{\mathcal{P}}_{(i)},\\ \hat{\Xi}_{12} \triangleq& -\big(\Omega_4^{(i)}\big)^T\tilde{\mathcal{P}}_{(i)}K^{(i)}M,\\ \hat{\Xi}_{13} \triangleq& \big(\Omega_4^{(i)}\big)^T\tilde{\mathcal{P}}_{(i)}K^{(i)},\\ \hat{\Xi}_{22} \triangleq& M^T\big(K^{(i)}\big)^T\tilde{\mathcal{P}}_{(i)}K^{(i)}M - \gamma_4 I,\\ \hat{\Xi}_{23} \triangleq& -M^T\big(K^{(i)}\big)^T\tilde{\mathcal{P}}_{(i)}K^{(i)},\\ \hat{\Xi}_{33} \triangleq& \big(K^{(i)}\big)^T\tilde{\mathcal{P}}_{(i)}K^{(i)} - \gamma_5 I.\end{aligned}$$

Utilizing the Schur Complement Lemma to (18) in Theorem 1 leads to

$$\Delta\mathcal{V}^+(k_\epsilon) < \gamma_4\upsilon^T(k_\epsilon)\upsilon^T(k_\epsilon) + \gamma_5\Phi^T(k_\epsilon)\Phi^T(k_\epsilon), \tag{28}$$

which implies

$$\mathbb{E}\{\mathcal{V}^+(k_\epsilon)\} <\rho_2\mathbb{E}\{\mathcal{V}(k_\epsilon)\} + \mu_2 \tag{29}$$

where

$$\mu_2 \triangleq \gamma_4\bar{\upsilon}^2 + \gamma_5\sum_{\jmath=1}^{N}\frac{n_y\delta_\jmath^2}{\lfloor\sqrt[n_y]{2^{U_\jmath}}\rfloor^2}.$$

In view of inequalities (26) and (29), the energy function can now be derived through a series of iterations over an arbitrary interval $(k_{\epsilon-1}, k_\epsilon]$ ($\epsilon \in \mathbb{N}^+$), and the following relations can be readily established:

$$\mathbb{E}\{\mathcal{V}(k)\} <\rho_1^k\mathbb{E}\{\mathcal{V}(0)\} + \sum_{\imath=0}^{k-1}\rho_1^\imath\mu_1,\ k \in (k_0, k_1],$$

$$\mathbb{E}\{\mathcal{V}^+(k_1)\} <\rho_1^{k_1}\rho_2\mathbb{E}\{\mathcal{V}(0)\} + \rho_2\sum_{\imath=0}^{k_1-1}\rho_1^\imath\mu_1 + \mu_2,$$

$$\begin{aligned}\mathbb{E}\{\mathcal{V}(k)\} <&\rho_1^k\rho_2\mathbb{E}\{\mathcal{V}(0)\} + \sum_{\imath=0}^{k-k_1-1}\rho_1^\imath\mu_1 + \rho_1^{k-k_1}\mu_2\\ &+ \rho_2\sum_{\imath=k-k_1}^{k-1}\rho_1^\imath\mu_1,\ k \in (k_1, k_2],\end{aligned}$$

$$\mathbb{E}\{\mathcal{V}^+(k_2)\} <\rho_1^{k_2}\rho_2^2\mathbb{E}\{\mathcal{V}(0)\} + \rho_2\sum_{\imath=0}^{k_2-k_1-1}\rho_1^\imath\mu_1$$

Citation information: DOI: 10.1109/TNNLS.2024.3448376, IEEE Transactions on Neural Networks and Learning Systems

$$
\begin{aligned}
&+\rho_2^2\sum_{\imath=k_2-k_1}^{k_2-1}\rho_1^\imath\mu_1+\rho_1^{k_2-k_1}\rho_2\mu_2+\mu_2,\\
\mathbb{E}\{\mathcal{V}(k)\}<&\rho_1^k\rho_2^2\mathbb{E}\{\mathcal{V}(0)\}+\rho_2\sum_{\imath=k-k_2}^{k-k_1-1}\rho_1^\imath\mu_1\\
&+\rho_2^2\sum_{\imath=k-k_1}^{k-1}\rho_1^\imath\mu_1+\rho_1^{k-k_1}\rho_2\mu_2\\
&+\rho_1^{k-k_2}\mu_2+\sum_{\imath=0}^{k-k_2-1}\rho_1^\imath\mu_1,\ k\in(k_2,k_3],
\end{aligned}
$$

and so on.

Over the interval $(k_{\epsilon-1},k_\epsilon]$, we utilize mathematical induction (a method of logical deduction) to calculate that

$$
\begin{aligned}
\mathbb{E}\{\mathcal{V}(k)\}<&\rho_1^k\rho_2^{\epsilon-1}\mathbb{E}\{\mathcal{V}(0)\}+\sum_{\imath=0}^{k-k_{\epsilon-1}-1}\rho_1^\imath\mu_1\\
&+\rho_2\sum_{\imath=k-k_{\epsilon-1}}^{k-k_{\epsilon-2}-1}\rho_1^\imath\mu_1+\ldots+\rho_2^{\epsilon-1}\sum_{\imath=k-k_1}^{k-1}\rho_1^\imath\mu_1\\
&+\rho_2^{\epsilon-2}\rho_1^{k-k_1}\mu_2+\rho_2^{\epsilon-3}\rho_1^{k-k_2}\mu_2+\ldots\\
&+\rho_2^0\rho_1^{k-k_{\epsilon-1}}\mu_2,\ k\in(k_{\epsilon-1},k_\epsilon].
\end{aligned}\tag{30}
$$

Furthermore, the coefficient ρ_1 in non-impulse instants is classified into the following two cases:

$$
\begin{cases}
\textbf{Case I}:\rho_1\ge 1,\ 0<\rho_2<1,\\
\textbf{Case II}:0<\rho_1<1,\ 0<\rho_2<1
\end{cases}\tag{31}
$$

according to which the Lyapunov-like function is analyzed separately.

For **Case I**, we derive from Assumption 2 that

$$
\begin{cases}
k-k_{\epsilon-1}<\tilde{\hbar}\\
k-k_{\epsilon-2}<2\tilde{\hbar}\\
\qquad\vdots\\
k-k_0<\epsilon\tilde{\hbar}.
\end{cases}\tag{32}
$$

The above amplification operation facilitates the analysis of (30), which gives rise to

$$
\begin{aligned}
&\mathbb{E}\{\mathcal{V}(k)\}\\
<&\rho_1^{\epsilon\tilde{\hbar}}\rho_2^{\epsilon-1}\mathbb{E}\{\mathcal{V}(0)\}+\sum_{\imath=0}^{\tilde{\hbar}-1}\rho_1^\imath\mu_1\\
&+\rho_2\sum_{\imath=\tilde{\hbar}}^{2\tilde{\hbar}-1}\rho_1^\imath\mu_1+\ldots+\rho_2^{\epsilon-1}\sum_{\imath=(\epsilon-1)\tilde{\hbar}}^{\epsilon\tilde{\hbar}-1}\rho_1^\imath\mu_1\\
&+\left(\rho_2^{\epsilon-2}\rho_1^{(\epsilon-1)\tilde{\hbar}}+\rho_2^{\epsilon-3}\rho_1^{(\epsilon-2)\tilde{\hbar}}+\ldots+\rho_2^0\rho_1^{\tilde{\hbar}}\right)\mu_2\\
=&\rho_1^{\epsilon\tilde{\hbar}}\rho_2^{\epsilon-1}\mathbb{E}\{\mathcal{V}(0)\}+\sum_{\imath=0}^{\tilde{\hbar}-1}\rho_1^\imath\mu_1\\
&+\rho_1^{\tilde{\hbar}}\rho_2\sum_{\imath=0}^{\tilde{\hbar}-1}\rho_1^\imath\mu_1+\ldots+\rho_1^{(\epsilon-1)\tilde{\hbar}}\rho_2^{\epsilon-1}\sum_{\imath=0}^{\tilde{\hbar}-1}\rho_1^\imath\mu_1\\
&+\left(\rho_2^{\epsilon-2}\rho_1^{(\epsilon-1)\tilde{\hbar}}+\rho_2^{\epsilon-3}\rho_1^{(\epsilon-2)\tilde{\hbar}}+\ldots+\rho_2^0\rho_1^{\tilde{\hbar}}\right)\mu_2\\
=&\rho_1^{\epsilon\tilde{\hbar}}\rho_2^{\epsilon-1}\mathbb{E}\{\mathcal{V}(0)\}+\Big(1+\rho_1^{\tilde{\hbar}}\rho_2+(\rho_1^{\tilde{\hbar}}\rho_2)^2+\ldots\\
&+\left(\rho_1^{\tilde{\hbar}}\rho_2\right)^{\epsilon-1}\Big)\sum_{\imath=0}^{\tilde{\hbar}-1}\rho_1^\imath\mu_1+\rho_1\mu_2\Big(\left(\rho_1^{\tilde{\hbar}}\rho_2\right)^{\epsilon-2}\\
&+\left(\rho_1^{\tilde{\hbar}}\rho_2\right)^{\epsilon-3}+\ldots+\rho_1^{\tilde{\hbar}}\rho_2+1\Big)+\rho_1^{\tilde{\hbar}}\mu_2-\rho_1\mu_2.
\end{aligned}\tag{33}
$$

According to the condition (19) and the Taylor expansion formula, we further have

$$
\begin{aligned}
\mathbb{E}\{\mathcal{V}(k)\}<&\rho_1\left(\rho_1^{\tilde{\hbar}}\rho_2\right)^{\epsilon-1}\mathbb{E}\{\mathcal{V}(0)\}+\left(\frac{1}{1-\rho_1^{\tilde{\hbar}}\rho_2}-1\right)\rho_1\mu_2\\
&+\rho_1^{\tilde{\hbar}}\mu_2+\frac{1}{1-\rho_1^{\tilde{\hbar}}\rho_2}\sum_{\imath=0}^{\tilde{\hbar}-1}\rho_1^\imath\mu_1,
\end{aligned}\tag{34}
$$

which implies

$$
\begin{aligned}
&\mathbb{E}\left\{\|e(k)\|^2\right\}\\
<&\frac{\rho_1\left(\rho_1^{\tilde{\hbar}}\rho_2\right)^{\epsilon-1}}{\min_{i\in\Pi}\underline{\lambda}\left(\mathcal{P}^{(i)}\right)}\mathbb{E}\{\mathcal{V}(0)\}\\
&+\frac{\left(\frac{1}{1-\rho_1^{\tilde{\hbar}}\rho_2}-1\right)\rho_1\mu_2+\rho_1^{\tilde{\hbar}}\mu_2+\frac{1}{1-\rho_1^{\tilde{\hbar}}\rho_2}\sum_{\imath=0}^{\tilde{\hbar}-1}\rho_1^\imath\mu_1}{\min_{i\in\Pi}\underline{\lambda}\left(\mathcal{P}^{(i)}\right)}.
\end{aligned}\tag{35}
$$

Furthermore, the following inequality

$$
\begin{aligned}
&\mathbb{E}\left\{\|e(k)\|^2\right\}\\
<&\frac{\left(\frac{1}{1-\rho_1^{\tilde{\hbar}}\rho_2}-1\right)\rho_1\mu_2+\rho_1^{\tilde{\hbar}}\mu_2+\frac{1}{1-\rho_1^{\tilde{\hbar}}\rho_2}\sum_{\imath=0}^{\tilde{\hbar}-1}\rho_1^\imath\mu_1}{\min_{i\in\Pi}\underline{\lambda}\left(\mathcal{P}^{(i)}\right)}\\
\triangleq&\mathcal{B}_1
\end{aligned}\tag{36}
$$

holds as k tends to infinity (i.e. $\epsilon\to\infty$).

In **Case II**, since $0<\rho_1<1$, the following relations are satisfied:

$$
\begin{cases}
k-k_{\epsilon-1}>0\\
k-k_{\epsilon-2}>\tilde{\hbar}\\
\qquad\vdots\\
k-k_0>(\epsilon-1)\tilde{\hbar}.
\end{cases}\tag{37}
$$

Similar to what we have derived in **Case I**, we obtain

$$
\begin{aligned}
&\mathbb{E}\{\mathcal{V}(k)\}\\
<&\rho_1^{(\epsilon-1)\tilde{\hbar}}\rho_2^{\epsilon-1}\mathbb{E}\{\mathcal{V}(0)\}+\rho_2\sum_{\imath=0}^{\tilde{\hbar}-1}\rho_1^\imath\mu_1+\rho_2^2\sum_{\imath=\tilde{\hbar}}^{2\tilde{\hbar}-1}\rho_1^\imath\mu_1\\
&+\ldots+\rho_2^{\epsilon-1}\sum_{\imath=(\epsilon-2)\tilde{\hbar}}^{(\epsilon-1)\tilde{\hbar}-1}\rho_1^\imath\mu_1+\Big(\rho_2^{\epsilon-2}\rho_1^{(\epsilon-2)\tilde{\hbar}}\\
&+\rho_2^{\epsilon-3}\rho_1^{(\epsilon-3)\tilde{\hbar}}+\ldots+\rho_2\rho_1^{\tilde{\hbar}}+1\Big)\mu_2\\
=&\left(\rho_1^{\tilde{\hbar}}\rho_2\right)^{\epsilon-1}\mathbb{E}\{\mathcal{V}(0)\}+\rho_2\sum_{\imath=0}^{\epsilon-2}\left(\rho_1^{\tilde{\hbar}}\rho_2\right)^\imath\sum_{\imath=0}^{\tilde{\hbar}-1}\rho_1^\imath\mu_1
\end{aligned}
$$

This article has been accepted for publication in a future issue of this journal, but has not been fully edited. Content may change prior to final publication.
Citation information: DOI: 10.1109/TNNLS.2024.3448376, IEEE Transactions on Neural Networks and Learning Systems

$$+\sum_{\imath=0}^{\epsilon-2}\left(\rho_1^{\tilde{\hbar}}\rho_2\right)^{\imath}\mu_2. \tag{38}$$

Combining (19) with (38), it follows from the fact of

$$\begin{aligned}&\mathbb{E}\left\{\|e(k)\|^2\right\}\\&<\frac{\left(\rho_1^{\tilde{\hbar}}\rho_2\right)^{\epsilon-1}}{\min_{i\in\Pi}\underline{\lambda}\left(\mathcal{P}^{(i)}\right)}\mathbb{E}\{\mathcal{V}(0)\}\\&\quad+\left(\frac{\mu_2}{1-\rho_1^{\tilde{\hbar}}\rho_2}+\frac{\rho_2}{1-\rho_1^{\tilde{\hbar}}\rho_2}\sum_{\imath=0}^{\tilde{\hbar}-1}\rho_1^{\imath}\mu_1\right)\Big/\min_{i\in\Pi}\underline{\lambda}\left(\mathcal{P}^{(i)}\right)\end{aligned} \tag{39}$$

that the following relationship

$$\begin{aligned}&\mathbb{E}\left\{\|e(k)\|^2\right\}\\&<\left(\frac{\mu_2}{1-\rho_1^{\tilde{\hbar}}\rho_2}+\frac{\rho_2}{1-\rho_1^{\tilde{\hbar}}\rho_2}\sum_{\imath=0}^{\tilde{\hbar}-1}\rho_1^{\imath}\mu_1\right)\Big/\min_{i\in\Pi}\underline{\lambda}\left(\mathcal{P}^{(i)}\right)\\&\triangleq\mathcal{B}_2\end{aligned} \tag{40}$$

is true when time k tends to infinity.

Based on Definition 1, the error dynamics is determined to be exponentially mean-square bounded. Referring to formulas (36) and (40), it can be inferred that $\mathcal{B}_2<\mathcal{B}_1$, which indicates that a lower convergence coefficient ρ_1 during the non-impulse interval results in a quicker convergence rate of the error dynamics $e(k)$ and, consequently, a reduced error upper bound (EUB). Thus, the proof is concluded. ■

Remark 4: The theoretical advantages of an impulsive observer over a traditional one can be analyzed by comparing their respective observer structures and energy functions. In the absence of an impulse mechanism, the observer (9) is modified to:

$$\begin{aligned}\hat{x}_\jmath(k)=&A_\jmath\hat{x}_\jmath(k-1)+\sum_{\jmath=1}^{N}\omega_{\jmath\ell}^{\sigma(k-1)}\Gamma\hat{x}_\ell(k-1)\\&+B_\jmath f(\hat{x}_\jmath(k-1))+\left(L_\jmath^{\sigma(k-1)}+\Delta L_\jmath(k-1)\right)\\&\times\left(\vec{y}_\jmath(k-1)-C_\jmath\hat{x}_\jmath(k-1)\right).\end{aligned}$$

The corresponding energy function, shown as (26), is deduced to be:

$$\begin{aligned}\mathbb{E}\{\mathcal{V}(k)\}<&\rho_1\mathbb{E}\{\mathcal{V}(k-1)\}+\mu_1<\cdots\\<&\rho_1^k\mathbb{E}\{\mathcal{V}(0)\}+\sum_{\imath=0}^{k-1}\rho_1^{\imath}\mu_1.\end{aligned}$$

Comparing this to the impulsive approach (30), it is evident that the coefficient $\rho_1^k\rho_2^{\epsilon-1}$ of energy function (30) is less than ρ_1^k in the non-impulsive case, which means that the former case converges faster. For visual clarity, Fig. 1 conceptually illustrates the decay of the energy function $\mathbb{E}\{\mathcal{V}(k)\}$ for both scenarios, showing the efficiency of the impulsive mechanism in enhancing convergence.

Remark 5: Based on the forms $\mathcal{B}_1$ and $\mathcal{B}_2$ of the estimation error bound, we can conclude that the EUB is influenced by various factors including bounded noise, coding-decoding parameters $\delta_\jmath$, bit rate $U_\jmath$, maximum impulse interval $\tilde{\hbar}$, and convergence coefficients ρ_1 and ρ_2. When all system parameters, $\delta_\jmath$ and $\tilde{\hbar}$ are fixed, the EUB is directly associated with the bit rate $U_\jmath$ of each node. Specifically, an increase in $U_\jmath$ leads to a higher maximum quantization level $\hat{q}_\jmath$, resulting in lower decoding errors and a consequent decrease in the EUB. This relationship underscores the critical role of bit rate in reducing estimation errors in digital communication networks.

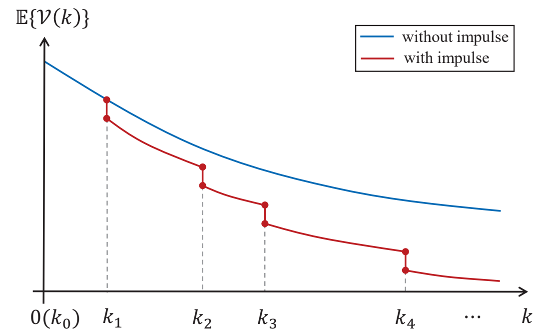

Fig. 1. Energy function with and without impulse mechanism.

B. Impulsive Observer Gain Design

Having analyzed the boundedness of the error dynamics, the next step would be to focus on the design of impulsive observer gains by taking into account the specified bit rate allocation.

Theorem 2: Consider the CN (1) and the impulsive observer (9) with known positive integers $U_\jmath$ and let the scalars $\rho_1>0$, $0<\rho_2<1$, $\tilde{\hbar}\geq 1$ be given. Then, the estimation error dynamics is exponentially mean-square bounded if there exist positive scalars $\alpha_1,\alpha_2,\alpha_3,\gamma_\iota>0$ ($\iota\in\{1,2,\ldots,5\}$), positive definite non-singular matrices $P_\jmath^{(i)}$ ($\jmath\in\mathcal{J}$), and observer gain matrices $L_\jmath^{(i)}$, $K_\jmath^{(i)}$ ($\jmath\in\mathcal{J}$) such that the following inequalities and (19) hold for all $i\in\Pi$:

$$\begin{bmatrix}\hat{\Omega}_1^{(i)}&\hat{\Omega}_2^{(i)}&0\\ *&-\tilde{\mathcal{P}}_{(i)}^T&\hat{\Omega}_3^{(i)}\\ *&*&\hat{\Omega}_4\end{bmatrix}<0 \tag{41}$$

$$\begin{bmatrix}-\rho_2\tilde{\mathcal{P}}_{(i)}&0&0&\tilde{\mathcal{P}}_{(i)}^T-C^T\left(\mathcal{K}^{(i)}\right)^T\\ *&-\gamma_4 I&0&-M^T\left(\mathcal{K}^{(i)}\right)^T\\ *&*&-\gamma_5 I&\left(\mathcal{K}^{(i)}\right)^T\\ *&*&*&-\tilde{\mathcal{P}}_{(i)}^T\end{bmatrix}<0 \tag{42}$$

where

$$\hat{\Omega}_1^{(i)}\triangleq\begin{bmatrix}\hat{\Omega}_{11}^{(i)}&-\Lambda_2&0&0\\ *&-\gamma_1 I&0&0\\ *&*&\hat{\Omega}_{33}&0\\ *&*&*&\hat{\Omega}_{44}\end{bmatrix},$$

$$\hat{\Omega}_2^{(i)}\triangleq\left[\hat{\Omega}_{15}^{(i)}\quad\tilde{\mathcal{P}}_{(i)}B\quad\tilde{\mathcal{P}}_{(i)}S-\mathcal{L}^{(i)}M\quad\mathcal{L}^{(i)}\right]^T,$$

$$\hat{\Omega}_{11}^{(i)}\triangleq-\rho_1\mathcal{P}^{(i)}-\Lambda_1+\alpha_1 C^T H^T HC,$$

This article has been accepted for publication in a future issue of this journal, but has not been fully edited. Content may change prior to final publication.
Citation information: DOI: 10.1109/TNNLS.2024.3448376, IEEE Transactions on Neural Networks and Learning Systems

$$
\begin{aligned}
\hat{\Omega}_{33} &\triangleq -\gamma_2 I + \alpha_2 M^T H^T H M, \\
\hat{\Omega}_{44} &\triangleq -\gamma_3 I + \alpha_2 H^T H, \\
\hat{\Omega}_{15}^{(i)} &\triangleq \tilde{\mathcal{P}}_{(i)} A + \tilde{\mathcal{P}}_{(i)} (W^{(i)} \otimes \Gamma) - \mathcal{L}^{(i)} C, \\
\hat{\Omega}_{3}^{(i)} &\triangleq \begin{bmatrix} \tilde{\mathcal{P}}_{(i)} D & \tilde{\mathcal{P}}_{(i)} D & \tilde{\mathcal{P}}_{(i)} D \end{bmatrix}, \\
\hat{\Omega}_{4} &\triangleq \mathrm{diag}\{-\alpha_1 I, -\alpha_2 I, -\alpha_3 I\}.
\end{aligned}
$$

Moreover, the impulsive observer gains are given by

$$
L^{(i)} = \tilde{\mathcal{P}}_{(i)}^{-1} \mathcal{L}^{(i)}, \; K^{(i)} = \tilde{\mathcal{P}}_{(i)}^{-1} \mathcal{K}^{(i)}, \; i \in \Pi. \tag{43}
$$

Proof: Utilizing Lemma 1, we know that the condition (17) holds if and only if the following is true:

$$
\begin{aligned}
&\begin{bmatrix}
-\rho_1 \mathcal{P}^{(i)} - \Lambda_1 & -\Lambda_2 & 0 & 0 & \mathcal{O}_1^{(i)} \\
* & -\gamma_1 I & 0 & 0 & B^T \\
* & * & -\gamma_2 I & 0 & \mathcal{O}_2^{(i)} \\
* & * & * & -\gamma_3 I & L^T \\
* & * & * & * & -\tilde{\mathcal{P}}_{(i)}^{-1}
\end{bmatrix} \\
&+\alpha_1 \begin{bmatrix} -HC & 0 & 0 & 0 & 0 \end{bmatrix}^T \begin{bmatrix} -HC & 0 & 0 & 0 & 0 \end{bmatrix} \\
&+\alpha_2 \begin{bmatrix} 0 & 0 & -HM & 0 & 0 \end{bmatrix}^T \begin{bmatrix} 0 & 0 & -HM & 0 & 0 \end{bmatrix} \\
&+\alpha_3 \begin{bmatrix} 0 & 0 & 0 & H & 0 \end{bmatrix}^T \begin{bmatrix} 0 & 0 & 0 & H & 0 \end{bmatrix} \\
&+\left(\frac{1}{\alpha_1} + \frac{1}{\alpha_2} + \frac{1}{\alpha_3} \right) \begin{bmatrix} 0 & 0 & 0 & 0 & D^T \end{bmatrix}^T \\
&\times \begin{bmatrix} 0 & 0 & 0 & 0 & D^T \end{bmatrix} < 0, \; \forall i \in \Pi
\end{aligned} \tag{44}
$$

where

$$
\begin{aligned}
\mathcal{O}_1^{(i)} &\triangleq A^T + (W^{(i)} \otimes \Gamma)^T - C^T \left(L^{(i)} \right)^T, \\
\mathcal{O}_2^{(i)} &\triangleq S^T - M^T \left(L^{(i)} \right)^T.
\end{aligned}
$$

Applying the Schur Complement Lemma to the above inequality, we obtain

$$
\begin{bmatrix}
\hat{\Omega}_1^{(i)} & \mathcal{O}_3^{(i)} & 0 \\
* & -\tilde{\mathcal{P}}_{(i)}^{-1} & \mathcal{O}_4 \\
* & * & \hat{\Omega}_4
\end{bmatrix} < 0 \tag{45}
$$

where

$$
\begin{aligned}
\mathcal{O}_3^{i} &\triangleq \begin{bmatrix} \left(\mathcal{O}_1^{(i)}\right)^T & B & \left(\mathcal{O}_2^{(i)}\right)^T & L^{(i)} \end{bmatrix}^T, \\
\mathcal{O}_4 &\triangleq \begin{bmatrix} D & D & D \end{bmatrix}.
\end{aligned}
$$

Define

$$
\begin{aligned}
\mathcal{I}_1 &\triangleq \mathrm{diag}\{I, I, I, I, \tilde{\mathcal{P}}_{(i)}, I, I\}, \\
\mathcal{I}_2 &\triangleq \mathrm{diag}\{I, I, I, \tilde{\mathcal{P}}_{(i)}\}.
\end{aligned}
$$

By pre-multiplying the matrix in (45) with $\mathcal{I}_1$ and post-multiplying it with $\mathcal{I}_1^T$, we can conclude that the condition (41) holds. Similarly, (42) is established utilizing the operation of $\mathcal{I}_2$. The proof is now complete. ■

C. Co-design of Bit Rate Allocation Strategy and Observer

The allocation of specific bit rates to each node in CNs plays a critical role in determining the observer gains, as detailed in Theorem 2. Equations (36) and (40) make it clear that under fixed system parameters and quantization regions, the bit rate $U_\jmath$ significantly influences the upper bound of the error dynamics and, subsequently, the overall estimation performance. The main focus of this section is to further reduce the upper bound of the error dynamics, which is pursued by formulating an optimization problem that involves co-designing the bit rate allocation strategy along with the observer gains.

Based on Theorem 2, in the following corollary, we take the worst case (i.e., **Case I**) for optimization where (36) is satisfied.

Corollary 1: When the assigned bit rate $U_\jmath$ is a variable (to be designed), the optimization for the upper bound of the error dynamics is transformed into the following minimization problem:

$$
\begin{aligned}
&\min \; \frac{\mathcal{G}_1 \mu_2 + \mathcal{G}_2 \mu_1}{\min_{i \in \Pi} \underline{\lambda}\left(\mathcal{P}^{(i)}\right)} \\
&\text{s.t.} \;\; (3), \; (19), \; (41), \; (42), \; 0 \leq U_\jmath \leq U, \; \forall i \in \Pi
\end{aligned} \tag{46}
$$

where

$$
\begin{aligned}
\mathcal{G}_1 &\triangleq \left(\frac{1}{1 - \rho_1^{\tilde{\hbar}} \rho_2} - 1 \right) \rho_1 + \rho_1^{\tilde{\hbar}} \\
\mathcal{G}_2 &\triangleq \frac{1}{1 - \rho_1^{\tilde{\hbar}} \rho_2} \sum_{\imath=0}^{\tilde{\hbar}-1} \rho_1^{\imath}.
\end{aligned}
$$

Within this framework, the observer gains are derived by $L^{(i)} = \tilde{\mathcal{P}}_{(i)}^{-1} \mathcal{L}^{(i)}, \; K^{(i)} = \tilde{\mathcal{P}}_{(i)}^{-1} \mathcal{K}^{(i)}, \; i \in \Pi$.

Proof: The proof is similar to Theorem 2 and is omitted here for space saving. ■

Addressing the non-convex nature of the minimization problem presented in (46), which poses significant challenges in terms of solvability, requires an innovative approach. To tackle this issue, a co-design method is proposed that integrates the particle swarm optimization (PSO) algorithm with the linear matrix inequality (LMI) technique.

The minimization problem (46) involves constraints $0 \leq U_\jmath \leq U$ and (3). To effectively handle these constraints within the optimization process, a transformation of (46) is undertaken by introducing a penalty function:

$$
\begin{aligned}
&\min \; \frac{\mathcal{G}_1 \mu_2 + \mathcal{G}_2 \mu_1}{\min_{i \in \Pi} \underline{\lambda}\left(\mathcal{P}^{(i)}\right)} + \mathfrak{f} \mathcal{F}(\tilde{U}) \\
&\text{s.t.} \;\; (19), \; (41), \; (42), \; \forall i \in \Pi
\end{aligned} \tag{47}
$$

where $\mathcal{F}(\tilde{U}) \triangleq \max\left\{0, \sum_{\jmath=1}^{N} U_\jmath - U\right\}$ is the exterior penalty function with $\tilde{U} \triangleq [U_1, U_2, \ldots, U_N]$, and $\mathfrak{f}$ is a constant called penalty coefficient. The fitness function of PSO algorithm is the upper bound of the error dynamics, which is defined as

$$
\mathbf{F}(\tilde{U}) \triangleq \frac{\mathcal{G}_1 \mu_2 + \mathcal{G}_2 \mu_1}{\min_{i \in \Pi} \underline{\lambda}\left(\mathcal{P}^{(i)}\right)} + \mathfrak{f} \mathcal{F}(\tilde{U}).
$$

The observer design framework, as depicted in Fig. 2, illustrates the integration of the PSO algorithm with the LMI

This article has been accepted for publication in a future issue of this journal, but has not been fully edited. Content may change prior to final publication.
Citation information: DOI: 10.1109/TNNLS.2024.3448376, IEEE Transactions on Neural Networks and Learning Systems

technique based on the specified objective function. This algorithm is tailored to address the minimization problem by taking into account the constraints and nonlinearity inherent in the problem. In the PSO algorithm, a swarm of particles, each representing a potential solution, navigates through the search space. The position and velocity of each particle characterize these potential solutions. The algorithm operates by iteratively adjusting the positions of the particles. This adjustment is based not only on each particle's own experience but also on insights gleaned from the best-performing particles in the population. Through this process, the PSO algorithm efficiently searches for the optimal solution to the minimization problem, leveraging both individual and collective intelligence within the swarm.

We denote $\mathbf{X}_o \triangleq [\mathbf{X}_{o,1}, \mathbf{X}_{o,2}, \ldots, \mathbf{X}_{o,N}]$ and $\mathbf{V}_o \triangleq [\mathbf{V}_{o,1}, \mathbf{V}_{o,2}, \ldots, \mathbf{V}_{o,N}]$ $(o \in \{1, 2, \ldots \mathbf{N}\})$ as the position and velocity of the o-th particle, respectively. $\mathbf{N}$ is the number of particles in the search space, and the maximum number of iterations is represented by $\mathbf{I}$. The updates of particle velocity and position obey the following equations:

$$\begin{aligned}\mathbf{V}_o(\varrho+1) =&\mathbf{w}\mathbf{V}_o(\varrho) + \mathbf{c_1}\xi_1\big(\mathbf{P}_o(\varrho) - \mathbf{X}_o(\varrho)\big)\\ &+ \mathbf{c_2}\xi_2\big(\mathbf{P}_g(\varrho) - \mathbf{X}_o(\varrho)\big), \qquad (48)\\ \mathbf{X}_o(\varrho+1) =&\mathbf{X}_o(\varrho) + \mathbf{V}_o(\varrho) \qquad (49)\end{aligned}$$

where $\varrho \in \{1, 2, \ldots, \mathbf{I}\}$ indicates the iteration number; $\mathbf{w}$ stands for the inertia weight; the acceleration constants $\mathbf{c_1}$ and $\mathbf{c_2}$ denote the self-learning factor and the group learning factor, respectively; ξ_1 and ξ_2 are two stochastic integers distributed in the interval $[1, 2]$. To prevent the particle's search position from exceeding the limited interval leading to an unproductive blind search, well-defined boundaries are established for both position and velocity. These boundaries, denoted as $\mathbf{X}_T$ (upper bound), $\mathbf{X}_L$ (lower bound) for position, as well as $\mathbf{V}_T$ (upper bound), $\mathbf{V}_L$ (lower bound) for velocity, serve to confine the particle's movement within a controlled and purposeful range.

In Fig. 2, we first initialize parameters $\mathbf{N}, \mathbf{I}, \mathbf{w}, \mathbf{c_1}, \mathbf{c_2}$, the initial position $\mathbf{X}_o$ and the initial velocity $\mathbf{V}_o$ of each particle. Then, compute the fitness function $\mathbf{F}(\mathbf{X}_o)$ if LMIs (41) and (42) have feasible solution, otherwise, set $\mathbf{F}(\mathbf{X}_o) = \infty$. Next, update the velocity and position of the particle swarm according to formulas (48) and (49), and correct it based on the boundary constraints. Using the updated positions of the particles, we obtain the fitness function $\mathbf{F}(\text{new}\mathbf{X}_o)$ if $\mathbf{F}(\text{new}\mathbf{X}_o) < \mathbf{F}(\mathbf{X}_o)$ and there are feasible solutions for (41) and (42), and record the corresponding position $\mathbf{P}_o$. Subsequently, search for the historical minimum fitness and the corresponding position $\mathbf{P}_g$ in this iteration, and re-update position and velocity of the particle swarm until the iteration is terminated. Finally, the observer gains $L^{(i)}$ and $K^{(i)}$ are obtained by solving (41) and (42) under the optimal bit rate allocation protocol (i.e. position $\mathbf{P}_g$).

Through the PSO-based co-design method for observers, we achieve the optimal allocation strategy. This enables a thorough analysis of how varying bit rates impact the estimation performance of CNs.

Remark 6: Thus far, the impulsive estimation problem has been explored for discrete-time CNs with Markovian switching topologies within the context of digital communication networks. A significant focus has been placed on developing a model that takes into account the constraints posed by limited bit rates, reflecting the challenges of restricted transmission environments in digital networks. A key achievement of this study is the establishment of a sufficient condition, as presented in Theorem 1, which ensures the mean-square boundedness of the impulsive error dynamics. Furthermore, Theorem 2 has addressed the determination of impulsive observer gains under a given bit rate allocation. Moreover, to enhance the estimation performance by minimizing the upper bound of errors, Corollary 1 has attained a co-design of bit-rate allocation strategy and optimal observer gains.

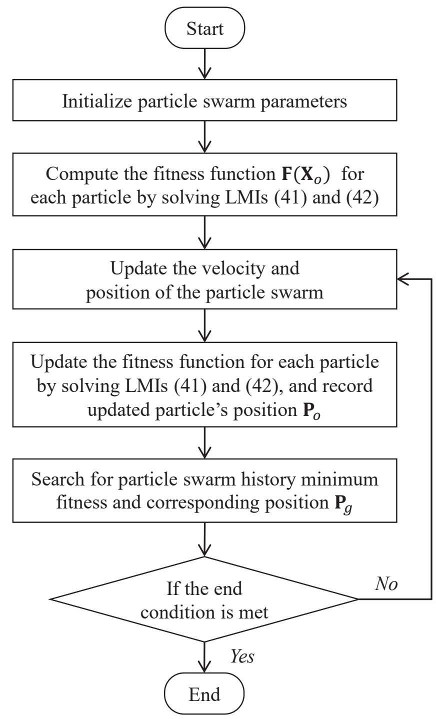

Fig. 2. Flowchart of the collaborative PSO algorithm.

Remark 7: In contrast to existing research on state estimation for CNs [11], [32], this paper introduces several key innovations: 1) the discrete-time CNs with Markovian switching topologies is first addressed in the context of digital communication networks, where the constrained bit rate of the wireless network is considered as a crucial factor; 2) within the established theoretical framework, a mode-dependent non-fragile impulsive observer is designed. The upper bound of the impulsive error dynamics is derived through a rigorous analysis of the Lyapunov-like function on the impulse-jump points; and 3) through the utilization of a PSO algorithm, we focus on minimizing the objective function that encompasses the upper bound of error dynamics. The co-design approach involving observer gains and bit-rate allocation protocol is proposed to enhance the estimation performance.

IV. Illustrative Example

In this section, a simulation example is presented to demonstrate the effectiveness of the impulsive observer under con-

This article has been accepted for publication in a future issue of this journal, but has not been fully edited. Content may change prior to final publication.
Citation information: DOI: 10.1109/TNNLS.2024.3448376, IEEE Transactions on Neural Networks and Learning Systems

strained bit rates.

We consider the CNs composed of $\jmath = 4$ nodes with three jumping topologies (i.e., $\Pi = \{1, 2, 3\}$). The system model parameters are given as follows:

$$A_1 = \begin{bmatrix} 0.55 & 0.13 \\ 0.15 & 0.51 \end{bmatrix}, \ A_2 = \begin{bmatrix} 0.6 & 0.2 \\ 0.1 & 0.45 \end{bmatrix},$$
$$A_3 = \begin{bmatrix} 0.4 & 0.15 \\ 0.2 & 0.62 \end{bmatrix}, \ A_4 = \begin{bmatrix} 0.5 & 0.1 \\ 0.13 & 0.35 \end{bmatrix},$$
$$B_1 = \begin{bmatrix} 0.3 & 0.3 \\ 0.2 & 0.2 \end{bmatrix}, \ B_2 = \begin{bmatrix} 0.2 & 0.1 \\ 0.3 & 0.25 \end{bmatrix},$$
$$B_3 = \begin{bmatrix} 0.15 & 0.2 \\ 0.15 & 0.25 \end{bmatrix}, B_4 = \begin{bmatrix} 0.23 & 0.12 \\ 0.2 & 0.35 \end{bmatrix},$$
$$C_1 = \begin{bmatrix} 0.3 & 0 \\ 0 & 0.8 \end{bmatrix}, \ C_2 = \begin{bmatrix} 0.5 & 0 \\ 0 & 0.6 \end{bmatrix},$$
$$C_3 = \begin{bmatrix} 0.8 & 0 \\ 0 & 1 \end{bmatrix}, \ C_4 = \begin{bmatrix} 0.6 & 0.2 \\ 0 & 1 \end{bmatrix},$$
$$D_1 = \mathrm{diag}\{1, 0.5\}, \ D_2 = \mathrm{diag}\{0.6, 0.7\},$$
$$D_3 = \mathrm{diag}\{0.5, 0.6\}, \ D_4 = \mathrm{diag}\{0.4, 0.6\},$$
$$H_1 = \mathrm{diag}\{0.3, 0.4\}, \ H_2 = \mathrm{diag}\{0.5, 0.2\},$$
$$H_3 = \mathrm{diag}\{0.6, 0.3\}, \ H_4 = \mathrm{diag}\{0.5, 0.5\},$$
$$Q_1(k) = \mathrm{diag}\{0.4, 0.5|\cos(k)|\},$$
$$Q_2(k) = \mathrm{diag}\{0.2, 0.3|\cos(k)|\},$$
$$Q_3(k) = \mathrm{diag}\{0.4|\sin(k)|, 0.5\},$$
$$Q_4(k) = \mathrm{diag}\{0.6, 0.4|\sin(k)|\}.$$

Let three jump topologies and inner coupling matrix be

$$W^{(1)} = \begin{bmatrix} -0.4 & 0.2 & 0 & 0.2 \\ 0.3 & -0.6 & 0.1 & 0.2 \\ 0.2 & 0 & -0.3 & 0.1 \\ 0.2 & 0.1 & 0.1 & -0.4 \end{bmatrix},$$
$$W^{(2)} = \begin{bmatrix} -0.6 & 0.2 & 0.2 & 0.2 \\ 0 & -0.3 & 0.2 & 0.1 \\ 0.1 & 0.2 & -0.4 & 0.1 \\ 0.3 & 0 & 0.2 & -0.5 \end{bmatrix},$$
$$W^{(3)} = \begin{bmatrix} -0.5 & 0.1 & 0.3 & 0.1 \\ 0.2 & -0.4 & 0.1 & 0.1 \\ 0.2 & 0.1 & -0.5 & 0.2 \\ 0.3 & 0 & 0.3 & -0.6 \end{bmatrix},$$
$$\Gamma = \begin{bmatrix} 0.19 & 0.1 \\ 0.4 & 0.2 \end{bmatrix}.$$

The nonlinear function $f(\cdot)$ is of the following form:

$$f(a) = 0.38\big(|a+1| - |a-1|\big).$$

The external noise is set as $\upsilon(k) = 0.3\cos(k)$, and the corresponding coefficient matrices are given by

$$M_1 = \begin{bmatrix} 0.12 & 0.1 \end{bmatrix}^T, \ M_2 = \begin{bmatrix} 0.1 & 0.12 \end{bmatrix}^T,$$
$$M_3 = \begin{bmatrix} 0.11 & 0.03 \end{bmatrix}^T, \ M_4 = \begin{bmatrix} 0.2 & 0.15 \end{bmatrix}^T,$$
$$S_1 = \begin{bmatrix} 0.23 & 0.31 \end{bmatrix}^T, \ S_2 = \begin{bmatrix} 0.25 & 0.23 \end{bmatrix}^T,$$
$$S_3 = \begin{bmatrix} 0.2 & 0.2 \end{bmatrix}^T, \ S_4 = \begin{bmatrix} 0.22 & 0.2 \end{bmatrix}^T.$$

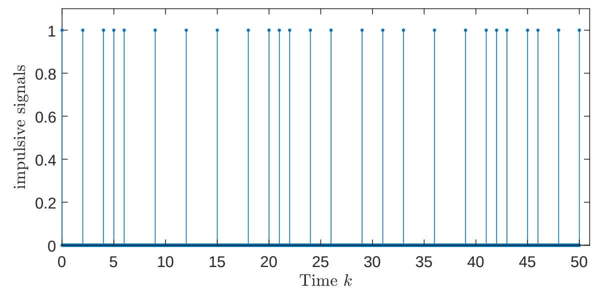

Fig. 3. The impulsive triggering signals.

Assuming that the maximum impulse triggering interval is $\tilde{\hbar} = 3$. The impulsive signals are shown in Fig. 3. The initial state and corresponding estimate are provided as

$$x_1(0) = \begin{bmatrix} 0.4 & 0.2 \end{bmatrix}^T, \ x_2(0) = -\begin{bmatrix} 0.2 & 0.2 \end{bmatrix}^T,$$
$$x_3(0) = \begin{bmatrix} 0.1 & 0.3 \end{bmatrix}^T, \ x_4(0) = -\begin{bmatrix} 0.2 & 0.3 \end{bmatrix}^T,$$
$$\hat{x}_1(0) = \begin{bmatrix} 0.1 & 0.3 \end{bmatrix}^T, \ \hat{x}_2(0) = \begin{bmatrix} 0.3 & 0.2 \end{bmatrix}^T,$$
$$\hat{x}_3(0) = \begin{bmatrix} 0.4 & 0.1 \end{bmatrix}^T, \ \hat{x}_4(0) = \begin{bmatrix} 0.2 & 0.3 \end{bmatrix}^T.$$

Based on the aforementioned parameter settings, the estimation performance of CNs is analyzed under impulse strategy and various bit rate allocation protocols.

Scenario 1: Firstly, we employ an average allocation strategy (AAS) to compute the gains of the impulsive observer. This strategy ensures that each node in the network is assigned with identical bit rates, thereby guaranteeing an equitable distribution of network resources. Based on Theorem 2, assume that $\rho_1 = 1.01$, $\rho_2 = 0.5$, and the available bit rates of the entire wireless network are $U = 60$. We have $U_1 = U_2 = U_3 = U_4 = \lfloor U/4 \rfloor = 15$ bps by AAS. The parameters $\delta_\jmath$ of the quantization region are chosen as $\delta_1 = 0.5, \ \delta_2 = 1, \ \delta_3 = 1.5, \ \delta_4 = 0.2$.

Due to the introduction of a Markovian switching topology, the error system exhibits stochastic behavior. We conducted $\acute{t} = 100$ repeated simulation experiments and obtain the average variables of the state, estimation, and error as $\bar{x}_\jmath(k) \triangleq \sum_{t=1}^{\acute{t}} x_\jmath^{(t)}(k)/\acute{t}$, $\tilde{x}_\jmath(k) \triangleq \sum_{t=1}^{\acute{t}} \hat{x}_\jmath^{(t)}(k)/\acute{t}$ and $\bar{e}_\jmath(k) \triangleq \sum_{t=1}^{\acute{t}} e_\jmath^{(t)}(k)/\acute{t}$, respectively. $x_\jmath^{(t)}(k)$, $\hat{x}_\jmath^{(t)}(k)$ and $e_\jmath^{(t)}(k)$ represent, respectively, the t-th simulation of $x_\jmath(k)$, $\hat{x}_\jmath(k)$ and $e_\jmath(k)$. Then, we plot the trajectories of state and corresponding estimate for the four nodes in Figs. 4-5.

To validate the advantages of the proposed impulsive observer in this work, we use $\bar{e}_n(k)$ to characterize the estimation error without impulse signal. Define $S(\|\bar{e}(k)\|) \triangleq \sum_{\hat{k}=1}^{k} \|\bar{e}(\hat{k})\|$ and $S(\|\bar{e}_n(k)\|) \triangleq \sum_{\hat{k}=1}^{k} \|\bar{e}_n(\hat{k})\|$ for visually illustrating the magnitude of estimation errors in both pulsing and non-pulsing scenarios. As depicted in Fig. 6, the sum of error norm $S(\|\bar{e}(k)\|)$ with the impulsive observer tends to be lower than that with the traditional observer.

This article has been accepted for publication in a future issue of this journal, but has not been fully edited. Content may change prior to final publication.
Citation information: DOI: 10.1109/TNNLS.2024.3448376, IEEE Transactions on Neural Networks and Learning Systems

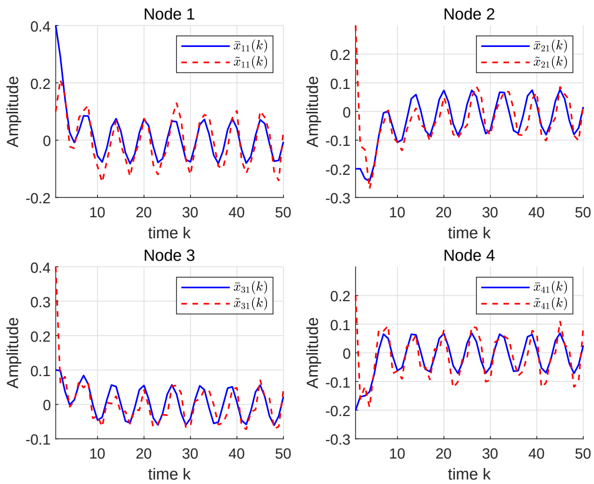

Fig. 4. Node state and estimation in the first dimension.

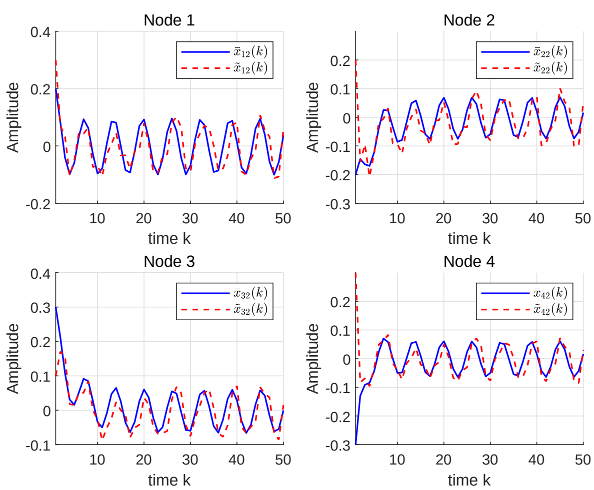

Fig. 5. Node state and estimation in the second dimension.

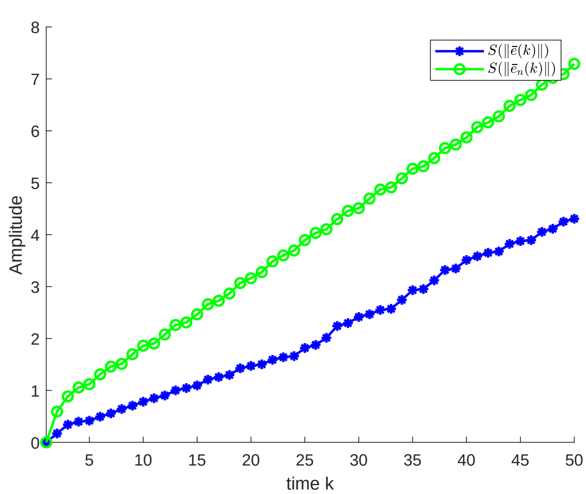

Fig. 6. Sum of error norm with and without impulsive signal.

TABLE I
EFFECT OF DIFFERENT MAXIMUM IMPULSE INTERVAL ON THE EUB

Maximum interval $\tilde{h}$	2	3	5	7
Upper bound $\sqrt{\mathcal{B}_1}$	2.0424	2.3865	2.9860	3.5128

TABLE II
EFFECT OF DIFFERENT PROTOCOLS ON THE EUB

U (bps)	Protocol	Bit rate allocation U_1, U_2, U_3, U_4 (bps)	EUB
60	AAS	15, 15, 15 15	2.3883
	PSO	14, 17, 18, 11	2.3865 (↓ 0.075%)
50	AAS	12, 12, 12, 12	2.413
	PSO	11, 14, 16, 9	2.3947 (↓0.758%)
40	AAS	10, 10, 10, 10	2.4957
	PSO	10, 11, 12, 7	2.4373 (↓ 2.34%)
30	AAS	7, 7, 7, 7	3.2041
	PSO	7, 9, 10, 4	2.6588 (↓ 17.019%)
20	AAS	5, 5, 5, 5	5.2774
	PSO	4, 6, 7, 3	3.8800 (↓ 26.479%)

Because impulse mechanism plays a role in promoting the convergence of the observer, denser impulse signals lead to faster convergence of the error dynamics. Therefore, the maximum interval $\tilde{h}$ of impulse triggering instants affects the estimation performance. Table I illustrates the relationship between the interval $\tilde{h}$ and the EUB $\sqrt{\mathcal{B}_1}$.

Scenario 2: In some specific application scenarios, adopting an AAS might not be the most optimal approach, because certain nodes may necessitate higher transmission speeds for carrying out more complex tasks compared to others. In such scenarios, to enhance the performance of the CNs, it is advisable to use the EUB as a metric and employ the PSO algorithm to dynamically adjust the bit rate allocation strategy. The superiority of the PSO-based bit rate allocation strategy over the AAS becomes evident through the following analysis.

Set the quantization-related parameters to be $\delta_1 = 0.5$, $\delta_2 = 1$, $\delta_3 = 1.5$ and $\delta_4 = 0.2$. We consider a range of available bit rates: 60, 50, 40, 30, and 20 bps. Both the AAS and PSO algorithm are employed to assess the estimation performance, and the results are summarized in Table II. It is evident from Table II that the PSO algorithm not only maximizes the utilization of network resources but also optimizes bit rate allocation based on the specific demands of each node, thereby enhancing the estimation performance for the CNs. Furthermore, it can be inferred that with increasing available bit rates U, the EUB gradually diminishes. This phenomenon arises from the fact that a higher number of bit rates leads to an enhanced uniform quantization resolution, subsequently reducing coding-decoding errors.

V. CONCLUSION

In this study, we have addressed the impulsive estimation problem within discrete-time CNs operating under the constraints of bit rates. A class of CNs characterized by Markovian

Citation information: DOI: 10.1109/TNNLS.2024.3448376, IEEE Transactions on Neural Networks and Learning Systems

switching topologies has been considered. The data transmission between nodes and the observer has been conducted through a digital network with limited bandwidth described by bit rate limitations. We have developed a mode-dependent nonfragile observer that leverages the power of the impulse mechanism, providing the observer with robustness and rapid convergence capabilities. Within this established framework, we have derived a sufficient condition for the mean-square boundedness of the error dynamics. Through the utilization of the LMI technique, the mode-dependent impulsive observer gains have been designed. Subsequently, the PSO algorithm has been employed to facilitate the collaborative design of the impulsive observer gains and the bit rate allocation strategy. Finally, the effectiveness of the proposed impulse mechanism has been demonstrated through a simulation example, and a detailed analysis of the connection between estimation performance and constrained bit rates has been conducted. Future work will be concerned with an extension of state estimation for the impulsive system under the limited bit rate constraint. The estimator becomes passive as a result of the impulsive dynamical behavior of the systems, which may provide a different perspective on the estimation performance.

REFERENCES

[1] S. Boccaletti, V. Latora, Y. Moreno, M. Chavez and D. Hwang, Complex networks: structure and dynamics, *Physics Reports*, vol. 424, pp. 175-308, Feb. 2006.

[2] R. Caballero-Águila, A. Hermoso-Carazo and J. Linares-Pérez, Networked fusion estimation with multiple uncertainties and time-correlated channel noise, *Information Fusion*, vol. 54, pp. 161-171, Feb. 2020.

[3] J. Cao, D. Ding, J. Liu, E. Tian, S. Hu and X. Xie, Hybrid-triggered-based security controller design for networked control system under multiple cyber attacks, *Information Sciences*, vol. 548, pp. 69-84, Feb. 2021.

[4] K. Chen, W. He, Q.-L. Han, M. Xue and Y. Tang, Leader selection in networks under switching topologies with antagonistic interactions, *Automatica*, vol. 142, art. no. 110334, Aug. 2022.

[5] R. Chen and Q. Ling, Event-triggered feedback stabilisation of switched linear systems under finite bit rates, *IET Control Theory & Applications*, vol. 14, no. 20, pp. 3428-3439, Feb. 2021.

[6] W.-H. Chen, H. He, X. Lu and X. Deng, Impulsive observer-based design for state estimation of a class of nonlinear singularly perturbed systems with discrete measurements, *Nonlinear Analysis: Hybrid Systems*, vol. 41, art. no. 101027, Aug. 2021.

[7] W.-H. Chen, X. Lu and W.-X. Zheng, Impulsive stabilization and impulsive synchronization of discrete-time delayed neural networks, *IEEE Transactions on Neural Networks and Learning Systems*, vol. 26, no. 4, pp. 734-748, Apr. 2015.

[8] D. Ciuonzo, A. Aubry and V. Carotenuto, Rician MIMO channel- and jamming-aware decision fusion, *IEEE Transactions on Signal Processing*, vol. 65, no. 15, pp. 3866-3880, Aug. 2017.

[9] D. Ding, Q.-L. Han, X. Ge and J. Wang, Secure state estimation and control of cyber-physical systems: a survey, *IEEE Transactions on Systems, Man, and Cybernetics: Systems*, vol. 51, no. 1, pp. 176-190, Jan. 2021.

[10] D. Ding, Z. Tang, J. H. Park, Y. Wang and Z. Ji, Dynamic self-triggered impulsive synchronization of complex networks with mismatched parameters and distributed delay, *IEEE Transactions on Cybernetics*, vol. 53, no. 2, pp. 887-899, Feb. 2022.

[11] P. Duan, G. Lv, Z. Duan and Y. Lv, Resilient state estimation for complex dynamic networks with system model perturbation, *IEEE Transactions on Control of Network Systems*, vol. 8, no. 1, pp. 135-146, Mar. 2021.

[12] Y. Guo, C. Liu, Y. Liu, R. Lu and T. Huang, Bounded synchronization for uncertain master-slave neural networks: an adaptive impulsive control approach, *Neural Networks*, vol. 162, pp. 288-296, May 2023.

[13] B. Han, L. Luo, G. Li and X. Jiang, Dynamic topology awareness and localization for power distribution networks considering non-gaussian noise, *IEEE Transactions on Power Delivery*, vol. 36, no. 4, pp. 2343-2353, Aug. 2021.

[14] M. Han, H.-K. Lam, F. Liu, Y. Tang, B. Han and H. Zhou, Stabilization analysis and impulsive controller design for positive interval type-2 polynomial fuzzy systems, *IEEE Transactions on Fuzzy Systems*, vol. 30, no. 9, pp. 3952-3966, Sept. 2022.

[15] N. Hou, J. Li, H. Liu, Y. Ge and H. Dong, Finite-horizon resilient state estimation for complex networks with integral measurements from partial nodes, *Science China Information Sciences*, vol. 65, no. 3, art. no. 132205, Mar. 2022.

[16] O. Jaramillo, B. Castillo-Toledo and S. Di Gennaro, Robust impulsive observer-based stabilization for uncertain nonlinear systems with sampled-output, *IEEE Control Systems Letters*, vol. 5, no. 3, pp. 845-850, Jul. 2021.

[17] J. William Helton, S. McCullough, M. Putinar and V. Vinnikov, Convex matrix inequalities versus linear matrix inequalities, *IEEE Transactions on Automatic Control*, vol. 54, no. 5, pp. 952-964, May 2009.

[18] J.-Y. Li, Z. Wang, R. Lu and Y. Xu, A component-based coding-decoding approach to set-membership filtering for time-varying systems under constrained bit rate, *Automatica*, vol. 152, art. no. 110874, Mar. 2023.

[19] N. Li, Q. Li and J. Suo, Dynamic event-triggered H_∞ state estimation for delayed complex networks with randomly occurring nonlinearities, *Neurocomputing*, vol. 421, pp. 97-104, Jan. 2021.

[20] X. Li, D.-W. Ho and J. Cao, Finite-time stability and settling-time estimation of nonlinear impulsive systems, *Automatica*, vol. 99, pp. 361-368, Jan. 2019.

[21] X. Li, D. Peng and J. Cao, Lyapunov stability for impulsive systems via event-triggered impulsive control, *IEEE Transactions on Automatic Control*, vol. 65, no. 11, pp. 4908-4913, Nov. 2020.

[22] X. Li, X. Yang and J. Cao, Interval impulsive observer for linear systems with aperiodic discrete measurements, *Automatica*, vol. 117, art. no. 108981, Jul. 2020.

[23] L. Liu, L. Ma, J. Guo, J. Zhang and Y. Bo, Distributed set-membership filtering for time-varying systems: a coding-decoding-based approach, *Automatica*, vol. 129, art. no. 109684, Jul. 2021.

[24] Q. Liu, Z. Wang, X. He and D. Zhou, Event-based distributed filtering over Markovian switching topologies, *IEEE Transactions on Automatic Control*, vol. 64, no. 4, pp. 1595-1602, Apr. 2018.

[25] Y. Liu and Q. Ling, Stabilizing bit rate conditions for a scalar linear event-triggered system with Markov dropouts, *Automatica*, vol. 146, art. no. 110635, Dec. 2022.

[26] Z.-W. Liu, G. Wen, X. Yu, Z.-H. Guan and T. Huang, Delayed impulsive control for consensus of multiagent systems with switching communication graphs, *IEEE Transactions on Cybernetics*, vol. 50, no. 7, pp. 3045-3055, Jul. 2020.

[27] J. Lu, B. Jiang and W.-X. Zheng, Potential impacts of delay on stability of impulsive control systems, *IEEE Transactions on Automatic Control*, vol. 67, no. 10, pp. 5179-5190, Oct. 2022.

[28] B. Nun, M. F. Umar, A. Karaki, M. B. Shadmand, S. Bayhan and H. Abu-Rub, Rank-based predictive control for community microgrids with dynamic topology and multiple points of common coupling, *IEEE Journal of Emerging and Selected Topics in Industrial Electronics*, vol. 3, no. 1, pp. 144-155, Jan. 2022.

[29] V.-T. Pham, N. Messai and N. Manamanni, Impulsive observer-based control in clustered networks of linear multi-agent systems, *IEEE Transactions on Network Science and Engineering*, vol. 7, no. 3, pp. 1840-1851, Jul. 2020.

[30] E. R. Pinto, E. G. Nepomuceno and A. S. L. O. Campanharo, Individual-based modelling of animal brucellosis spread with the use of complex networks, *International Journal of Network Dynamics and Intelligence*, vol. 1, no. 1, pp. 120-129, Dec. 2022.

[31] D. Rabehi, N. Meslem, A. El Amraoui and N. Ramdani, Interval impulsive observer for linear systems with aperiodic discrete measurements, *IEEE Transactions on Automatic Control*, vol. 66, no. 11, pp. 5407-5413, Nov. 2021.

[32] H. Shen, X. Hu, X. Wu, S. He and J. Wang, Generalized dissipative state estimation of singularly perturbed switched complex dynamic networks with persistent dwell-time mechanism, *IEEE Transactions on Systems, Man, and Cybernetics: Systems*, vol. 52, no. 3, pp. 1795-1806, Mar. 2022.

[33] Q. Song, G. Wen, D. Meng, Z.-W. Liu and F. Liu, Distributed impulsive control for signed networks of coupled harmonic oscillators with sampled positions, *IEEE Transactions on Control of Network Systems*, vol. 8, no. 1, pp. 111-122, Mar. 2021.

[34] S.-H. Strogatz, Exploring complex networks, *Nature*, vol. 410, no. 6825, pp. 268-276, Mar. 2001.

[35] Y. Sun, L. Li and D. W. C. Ho, Synchronization control of complex dynamical networks: invariant pinning impulsive controller with

Citation information: DOI: 10.1109/TNNLS.2024.3448376, IEEE Transactions on Neural Networks and Learning Systems

asynchronous actuation, *IEEE Transactions on Network Science and Engineering*, vol. 9, no. 6, pp. 4255-4265, Nov. 2022.

[36] X. Wan, Y. Li, Y. Li and M. Wu, Finite-time H_∞ state estimation for two-time-scale complex networks under stochastic communication protocol, *IEEE Transactions on Neural Networks and Learning Systems*, vol. 33, no. 1, pp. 25-36, Jan. 2022.

[37] J. Wang, G. Wen and Z. Duan, Distributed antiwindup consensus control of heterogeneous multiagent systems over Markovian randomly switching topologies, *IEEE Transactions on Automatic Control*, vol. 67, no. 11, pp. 6310-6317, Nov. 2022.

[38] S. Wang, Z. Wang, H. Dong and Y. Chen, A dynamic event-triggered approach to recursive nonfragile filtering for complex networks with sensor saturations and switching topologies, *IEEE Transactions on Cybernetics*, vol. 52, no. 10, pp. 11041-11054, Oct. 2022.

[39] L. Xie, Output feedback H_∞ control of systems with parameter uncertainty, *International Journal of Control*, vol. 63, no. 4, pp. 741-750, Feb. 2007.

[40] M. Xing, J. Lu, J. Qiu and H. Shen, Synchronization of complex dynamical networks subject to DoS attacks: an improved coding-decoding protocol, *IEEE Transactions on Cybernetics*, vol. 53, no. 1, pp. 102-113, Jun. 2023.

[41] L. Xu and S. Ge, Exponential ultimate boundedness of nonlinear stochastic difference systems with time-varying delays, *International Journal of Control*, vol. 88, no. 5, pp. 983-989, Jan. 2015.

[42] F. Yang, Q.-L. Han and Y. Liu, Distributed H_∞ state estimation over a filtering network with time-varying and switching topology and partial information exchange, *IEEE Transactions on Cybernetics*, vol. 49, no. 3, pp. 870-882, Mar. 2019.

[43] F. Yang, J. Li, H. Dong and Y. Shen, Proportional-integral-type estimator design for delayed recurrent neural networks under encoding-decoding mechanism, *International Journal of Systems Science*, vol. 53, no. 13, pp. 2729-2741, Oct. 2022.

[44] L. Yang, H. Rao, M. Lin, Y. Xu and P. Shi, Optimal sensor scheduling for remote state estimation with limited bandwidth: a deep reinforcement learning approach, *Information Sciences*, vol. 588, pp. 279-292, Apr. 2022.

[45] H. Yu and T. Chen, Event-triggered tracking control with filtered outputs and impulsive observers, *IEEE Transactions on Cybernetics*, vol. 52, no. 6, pp. 4981-4992, Jun. 2022.

[46] L. Yu, Y. Liu, Y. Cui, N. D. Alotaibi and F. E. Alsaadi, Intermittent dynamic event-triggered state estimation for delayed complex networks based on partial nodes, *Neurocomputing* , vol. 459 , pp. 59-69, Oct. 2021.

[47] Y. Zhang, L. Zou, Y. Wang and Y.-A. Wang, Estimator design for complex networks with encoding decoding mechanism and buffer-aided strategy: a partial-nodes accessible case, *ISA Transactions*, vol. 127, pp. 68-79, Aug. 2022.

[48] F. Zhu, J. H. Park and L. Peng, Adaptive event-triggered quantized communication-based distributed estimation over sensor networks with semi-Markovian switching topologies, *IEEE Transactions on Signal and Information Processing over Networks*, vol. 8, pp. 258-272, Mar. 2022.

Yuru Guo was born in Hubei province, China, in 1997. She received her B.S. degree from the school of electrical engineering, Nanjing Institute of Technology, Jiangsu, China, in 2019, majoring in Building Electricity and Intelligence. She is currently working toward the Ph.D. degree in Control Science and Engineering at Guangdong University of Technology, Guangzhou, China.

She was a Visiting Ph.D. student with the Department of Computer Science, Brunel University London, Uxbridge, U.K., from 2023 to 2024. Her research interests include networked control systems and impulsive control.

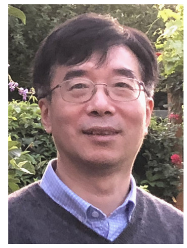

Zidong Wang (Fellow, IEEE) received the B.Sc. degree in mathematics in 1986 from Suzhou University, Suzhou, China, and the M.Sc. degree in applied mathematics in 1990 and the Ph.D. degree in electrical engineering in 1994, both from Nanjing University of Science and Technology, Nanjing, China.

He is currently a Professor of Dynamical Systems and Computing in the Department of Computer Science, Brunel University London, U.K. From 1990 to 2002, he held teaching and research appointments in universities in China, Germany and the U.K. Prof. Wang's research interests include dynamical systems, signal processing, bioinformatics, control theory and applications. He has published a number of papers in international journals. He is a holder of the Alexander von Humboldt Research Fellowship of Germany, the JSPS Research Fellowship of Japan, William Mong Visiting Research Fellowship of Hong Kong.

Prof. Wang serves (or has served) as the Editor-in-Chief for *International Journal of Systems Science*, the Editor-in-Chief for *Neurocomputing*, the Editor-in-Chief for *Systems Science & Control Engineering*, and an Associate Editor for 12 international journals including IEEE Transactions on Automatic Control, IEEE Transactions on Control Systems Technology, IEEE Transactions on Neural Networks, IEEE Transactions on Signal Processing, and IEEE Transactions on Systems, Man, and Cybernetics-Part C. He is a Member of the Academia Europaea, a Member of the European Academy of Sciences and Arts, an Academician of the International Academy for Systems and Cybernetic Sciences, a Fellow of the IEEE, a Fellow of the Royal Statistical Society and a member of program committee for many international conferences.

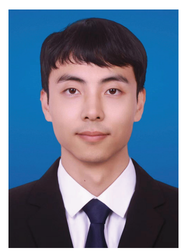

Jun-Yi Li was born in Henan province, China, in 1991. He received the M.S. degree in control science and engineering from Hangzhou Dianzi University, Hangzhou, China, in 2017 and the Ph.D. degree in Control Science and Engineering from Guangdong University of Technology, Guangzhou, China, in 2021. He is currently a Lecturer with the school of Automation, Guangdong University of Technology, Guangzhou, China.

He was a visiting Ph.D. student with the Department of Computer Science, Brunel University London, Uxbridge, U.K., from October 2019 to October 2020. His research interests include complex dynamical networks, networked systems.

Yong Xu (Member, IEEE) was born in Zhejiang Province, China, in 1983. He received the B.S. degree in information engineering from Nanchang Hangkong University, Nanchang, China, in 2007, the M.S. degree in control science and engineering from Hangzhou Dianzi University, Hangzhou, China, in 2010, and the Ph.D. degree in control science and engineering from Zhejiang University, Hangzhou, China, in 2014. He was a visiting internship student with the department of Electronic and Computer Engineering, Hong Kong University of Science and Technology, Hong Kong, China, from June 2013 to November 2013, where he was a Research Fellow from February 2018 to August 2018. Now he is a professor with School of Automation, at Guangdong University of Technology, Guangzhou, China.

His research interests include PID control, networked control systems, state estimation, and positive systems.